





This is to certify that the  
thesis entitled  
ROLE OF PHASE BOUNDARY ON DEFORMATION OF  
POLYCRYSTALLINE ALPHA-BETA BRASS

presented by

Sagar Prabhakar Naik

has been accepted towards fulfillment  
of the requirements for

       M.S.        degree in Material Science

*S. N. Subramanian*

\_\_\_\_\_  
Major professor

Date 11/15/85



RETURNING MATERIALS:

Place in book drop to  
remove this checkout from  
your record. FINES will  
be charged if book is  
returned after the date  
stamped below.

--	--	--

ROLE OF PHASE BOUNDARY ON DEFORMATION OF  
POLYCRYSTALLINE ALPHA-BETA BRASS

By

Sagar Prabhakar Naik

A THESIS

Submitted to  
Michigan State University  
in partial fulfillment of the requirements  
for the degree of

MASTER OF SCIENCE

Department of Metallurgy, Mechanics and Material Science

1985

## ABSTRACT

### ROLE OF PHASE BOUNDARY ON DEFORMATION OF POLYCRYSTALLINE ALPHA-BETA BRASS

By

Sagar Prabhakar Naik

The deformation structure near equiaxed phase boundary in polycrystalline specimens of two-phase alpha-beta brass was studied by Transmission Electron Microscopy after deforming the specimens up to a 27 percent strain level. Although dislocation pile-ups in alpha region were observed, no evidence of dislocation activity occurred as a result of this pile-up in beta phase near alpha-beta phase boundary. Dislocations observed in beta phase tended to be screw in character.

The Finite Element Method was used to study stress-strain relationship and stress-strain distribution in the region near the alpha-beta phase boundary. Increasing the number of elements incorporated in the chosen mesh increased the accuracy of the results obtained.

## ACKNOWLEDGMENTS

I would like to take this opportunity to sincerely thank my advisor, Dr. K. N. Subramanian, but for whose guidance and encouragement this endeavor would not have ended successfully.

A special thanks to my colleagues, Tong C. Lee, Narendra Dahotre, N. Krishnan, S. Sircar, S. Shekhar and Sanjeev Deshpande, for having helped me during this work. This work could not have been completed without the help of all the aforementioned.

## TABLE OF CONTENTS

List of Figures . . . . .	v
List of Tables . . . . .	x
I. INTRODUCTION . . . . .	1
II. HISTORICAL BACKGROUND . . . . .	4
II-A. Copper-Zinc System . . . . .	4
II-B. Deformation Behavior of Single Crystals of Alpha and Beta Brasses . . . . .	6
II-C. Deformation of Bicrystals of Alpha and Beta Brasses . . . . .	9
II-D. Deformation Behavior of Polycrystals of Alpha and Beta Brasses . . . . .	10
II-E. Deformation of Two-Phase Materials . . . . .	12
a) Deformation of Bicrystals of Two- Phase Materials	
b) Deformation of Polycrystals of Alpha-Beta Brass	
II-F. Theoretical Models for Interaction of Slip with Boundaries . . . . .	17
II-G. Finite Element Method . . . . .	18
III. EXPERIMENTAL PROCEDURE . . . . .	22
III-A. Procedures Used for Transmission Electron Microscopic Study of the Deformation Structure in the Phase Boundary Region . . . . .	22
III-B. Finite Element Analysis . . . . .	26
IV. RESULTS AND DISCUSSION . . . . .	37
IV-A. Transmission Electron Microscopic Analysis of the Deformation Structure in Alpha-Beta Brass . . . . .	37

a)	Analysis of Dislocations Present Near Phase Boundary	
b)	Interaction of Dislocations with Equiaxed Phase Boundary	
IV-B.	FEM Analysis of Stress-Strain Behavior of Alpha-Beta Brass . . . . .	73
a)	Stress-Strain Relationship for Alpha- Beta Brass Containing 25, 50, and 75 Volume Percent of Beta Phase	
b)	Stress-Strain Relationship for Small, Medium, and Coarse Grain Sizes of Alpha and Beta Phases	
c)	Stress-Strain Distribution Across Alpha-Beta Interface	
d)	Stress-Strain Curve for Two-Phase Region	
e)	Comparison of Experimental Stress- Strain Curve with the FEM-Calculated Curves (Two Different Meshes)	
V.	CONCLUSIONS . . . . .	94
V-A.	Transmission Electron Microscopic Studies . . . . .	94
V-B.	FEM Analysis . . . . .	94
VI.	REFERENCES . . . . .	95

## LIST OF FIGURES

Figure 1.	The copper-zinc phase diagram (Ref: 16) . . . . .	5
Figure 2.	Unit cell of ordered beta brass (A-Cu, B-Zn)(Ref: 19) . . . . .	7
Figure 3.	Schematic of "jet-polishing" unit . . . . .	24
Figure 4.	Schematic of the final electropolishing unit . . . . .	25
Figure 5.	FEM mesh for alpha-beta brass containing 25 volume percent beta phase (beta phase is shaded dark): . . . . . A) Fine grain distribution B) Medium grain distribution C) Coarse grain distribution	27
Figure 6.	FEM mesh for alpha-beta brass containing 50 volume percent beta phase (beta phase is shaded dark): . . . . . A) Fine grain distribution B) Medium grain distribution C) Coarse grain distribution	29
Figure 7.	FEM mesh for alpha-beta brass containing 75 volume percent beta phase (beta phase is shaded dark): . . . . . A) Fine grain distribution B) Medium grain distribution C) Coarse grain distribution	31
Figure 8.	FEM input stress-strain curve of "Alpha" and "Beta" brasses (Ref: 48) . . . . .	33
Figure 9.	FEM mesh, for alpha-beta brass containing 25 volume percent beta phase (shaded dark), used for calculation of the stress- strain distributions, across the alpha- beta interface . . . . .	35
Figure 10.	FEM mesh for alpha-beta brass containing 50 volume percent beta and 50 volume percent alpha . . . . . A) Phase boundary parallel to tensile axis B) Phase boundary perpendicular to tensile axis	36

Figure 11.	Dislocations near grain boundary in alpha phase of alpha-beta brass specimen deformed to 12 percent strain level . . . . .	39
	A) $g = [\bar{2}00]$	
	B) $g = [\bar{2}00]$	
	C) $g = [2\bar{2}0]$	
	D) $g = [2\bar{2}0]$	
	E) $g = [0\bar{2}0]$	
Figure 12.	Dislocations near grain boundary in alpha phase of alpha-beta brass. Location of grain boundary: upper right corner 60° to X-axis . . . . .	45
	A) $g = [1\bar{1}1]$	
	B) $g = [\bar{1}31]$	
	C) $g = [2\bar{2}0]$	
	D) $g = [042]$	
	Specimen deformed to 12 percent strain level	
Figure 13.	Dislocations near grain boundary in alpha phase of alpha-beta brass. Specimen deformed to 12 percent strain level . . .	47
	A) $g = [\bar{1}1\bar{1}]$	
	B) $g = [00\bar{2}]$	
	C) $g = [\bar{1}11]$	
Figure 14.	Dislocations in alpha region near alpha-beta phase boundary. Specimen deformed to 12 percent strain level. Location of phase boundary: lower left corner 50° to X-axis . . . . .	49
	A) $g = [00\bar{2}]$	
	B) $g = [\bar{1}11]$	
	C) $g = [1\bar{1}1]$	
Figure 15.	Dislocations in alpha region near alpha-beta phase boundary. Specimen deformed to 15 percent strain level . . . . .	53
	A) $g = [1\bar{1}1]$	
	B) $g = [\bar{1}11]$	
	C) $g = [00\bar{2}]$	
Figure 16.	Dislocations in alpha region near alpha-beta phase boundary. Specimen deformed to 15 percent strain level. Location of phase boundary: vertical, left . . . . .	57
	A) $g = [\bar{1}11]$	
	B) $g = [00\bar{2}]$	
	C) $g = [1\bar{1}1]$	

Figure 11.	Dislocations near grain boundary in alpha phase of alpha-beta brass specimen deformed to 12 percent strain level . . . . .	39
	A) $\vec{g} = [\bar{2}00]$	
	B) $\vec{g} = [\bar{2}00]$	
	C) $\vec{g} = [\bar{2}\bar{2}0]$	
	D) $\vec{g} = [\bar{2}\bar{2}0]$	
	E) $\vec{g} = [0\bar{2}0]$	
Figure 12.	Dislocations near grain boundary in alpha phase of alpha-beta brass. Location of grain boundary: upper right corner 60° to X-axis . . . . .	45
	A) $\vec{g} = [1\bar{1}1]$	
	B) $\vec{g} = [\bar{1}31]$	
	C) $\vec{g} = [\bar{2}\bar{2}0]$	
	D) $\vec{g} = [0\bar{4}2]$	
	Specimen deformed to 12 percent strain level	
Figure 13.	Dislocations near grain boundary in alpha phase of alpha-beta brass. Specimen deformed to 12 percent strain level . . .	47
	A) $\vec{g} = [\bar{1}1\bar{1}]$	
	B) $\vec{g} = [00\bar{2}]$	
	C) $\vec{g} = [\bar{1}11]$	
Figure 14.	Dislocations in alpha region near alpha-beta phase boundary. Specimen deformed to 12 percent strain level. Location of phase boundary: lower left corner 50° to X-axis . . . . .	49
	A) $\vec{g} = [00\bar{2}]$	
	B) $\vec{g} = [\bar{1}11]$	
	C) $\vec{g} = [1\bar{1}1]$	
Figure 15.	Dislocations in alpha region near alpha-beta phase boundary. Specimen deformed to 15 percent strain level . . . . .	53
	A) $\vec{g} = [1\bar{1}1]$	
	B) $\vec{g} = [\bar{1}11]$	
	C) $\vec{g} = [00\bar{2}]$	
Figure 16.	Dislocations in alpha region near alpha-beta phase boundary. Specimen deformed to 15 percent strain level. Location of phase boundary: vertical, left . . . . .	57
	A) $\vec{g} = [\bar{1}11]$	
	B) $\vec{g} = [00\bar{2}]$	
	C) $\vec{g} = [1\bar{1}1]$	

Figure 17.	Dislocations in alpha region near alpha-beta phase boundary. Specimen deformed to 18 percent strain level. Location of phase boundary: vertical, left . . . .	60
	A) $g = [1\bar{1}1]$	
	B) $g = [002]$	
	C) $g = [1\bar{1}1]$	
Figure 18.	Dislocations in beta region near alpha-beta phase boundary. Specimen strained to 18 percent strain level. Location of phase boundary: lower left corner $65^\circ$ to X-axis . . . . .	64
	A) $g = [200]$	
	B) $g = [110]$	
	C) $g = [1\bar{2}1]$	
	D) $g = [1\bar{1}0]$	
Figure 19.	Deformation structure near phase boundary of alpha-beta brass . . . . .	67
	A and B: Specimen deformed to 12 percent strain level	
	C and D: Specimen deformed to 15 percent strain level	
	E) Specimen deformed to 18 percent strain level	
	F) Specimen deformed to 20 percent strain level	
	G) Specimen deformed to 27 percent strain level	
Figure 20.	Antiphase boundaries in beta region of alpha-beta brass . . . . .	71
Figure 21.	FEM-calculated stress-strain curves for alpha-beta brass containing 25, 50, and 75 volume percents of beta phase. Grain size: small . . . . .	75
	I. % $V_\beta$ - 25%	
	II. % $V_\beta$ - 50%	
	III. % $V_\beta$ - 75%	
Figure 22.	FEM-calculated stress-strain curves of alpha-beta brass containing 25 volume percent beta phase for fine (I) and coarse (II) grain size distribution . . .	77
Figure 23.	FEM-calculated stress-strain curves of alpha-beta brass containing 50 volume percent beta phase for fine (I) and coarse (II) grain size distribution . . .	78

Figure 17.	Dislocations in alpha region near alpha-beta phase boundary. Specimen deformed to 18 percent strain level. Location of phase boundary: vertical, left . . . .	60
	A) $g = [1\bar{1}1]$	
	B) $g = [002]$	
	C) $g = [1\bar{1}1]$	
Figure 18.	Dislocations in beta region near alpha-beta phase boundary. Specimen strained to 18 percent strain level. Location of phase boundary: lower left corner $65^\circ$ to X-axis . . . . .	64
	A) $g = [200]$	
	B) $g = [110]$	
	C) $g = [1\bar{2}1]$	
	D) $g = [1\bar{1}0]$	
Figure 19.	Deformation structure near phase boundary of alpha-beta brass . . . . .	67
	A and B: Specimen deformed to 12 percent strain level	
	C and D: Specimen deformed to 15 percent strain level	
	E) Specimen deformed to 18 percent strain level	
	F) Specimen deformed to 20 percent strain level	
	G) Specimen deformed to 27 percent strain level	
Figure 20.	Antiphase boundaries in beta region of alpha-beta brass . . . . .	71
Figure 21.	FEM-calculated stress-strain curves for alpha-beta brass containing 25, 50, and 75 volume percents of beta phase. Grain size: small . . . . .	75
	I. % $V_\beta$ - 25%	
	II. % $V_\beta$ - 50%	
	III. % $V_\beta$ - 75%	
Figure 22.	FEM-calculated stress-strain curves of alpha-beta brass containing 25 volume percent beta phase for fine (I) and coarse (II) grain size distribution . . .	77
Figure 23.	FEM-calculated stress-strain curves of alpha-beta brass containing 50 volume percent beta phase for fine (I) and coarse (II) grain size distribution . . .	78

Figure 24.	FEM-calculated stress-strain curves of alpha-beta brass containing 75 volume percent beta phase for fine (I) and coarse (II) grain size distribution . . .	79
Figure 25.	FEM-calculated stress distribution plot in alpha and beta region of alpha-beta brass containing 25 volume percent beta phase in the Y-direction ( $\sigma_{yy}$ ) . . . . .	81
Figure 26.	FEM-calculated stress distribution plot in alpha and beta region of alpha-beta brass containing 25 volume percent beta phase, in the X-direction ( $\sigma_{xx}$ ) . . . . .	82
Figure 27.	FEM-calculated strain distribution plot in alpha and beta region of alpha-beta brass containing 25 volume percent beta phase . . . . .	84
Figure 28.	FEM-calculated stress distribution plot in alpha-beta region of alpha-beta brass containing 20 volume percent beta phase, in Y-direction ( $\sigma_{yy}$ ) . . . . . A) Stress distribution with 60-element mesh (Ref: 47) B) Stress distribution with 128-element mesh	85
Figure 29.	FEM-calculated stress distribution plot in alpha and beta region of alpha-beta brass containing 20 volume percent beta phase, in X-direction ( $\sigma_{xx}$ ) . . . . . A) Stress distribution with 60-element mesh (Ref: 47) B) Stress distribution with 128-element mesh	86
Figure 30.	FEM-calculated strain distribution plot in alpha and beta region of alpha-beta brass containing 20 volume percent beta phase . . . . . A) Strain distribution with 60-element mesh (Ref: 47) B) Strain distribution with 128-element mesh	87
Figure 31.	FEM-generated stress contour distribution plot in the 128-element mesh for alpha-beta brass containing 25 volume percent beta phase in the loading Y-direction ( $\sigma_{yy}$ ) . . . . .	88

Figure 32.	FEM-generated stress contour distribution plot in the 128-element mesh for alpha-beta brass containing 25 volume percent beta phase, in the X-direction ( $\sigma_{xx}$ ) . . .	89
Figure 33.	FEM-calculated stress-strain curves of alpha-beta brass containing 50 volume percent of alpha and 50 volume percent beta . . . . . I. Phase boundary parallel to tensile axis II. Phase boundary perpendicular to tensile axis	90
Figure 34.	FEM-calculated stress-strain curve of alpha-beta brass containing 80 volume percent of alpha and 20 volume percent beta . . . . . I. Phase boundary parallel to tensile axis II. Experimental III. Phase boundary perpendicular to the tensile axis	91
Figure 35.	Comparison between the experimentally determined stress-strain curve of 60 Cu-40 Zn brass and the FEM-calculated curves of alpha-beta brass containing 20 volume percent beta phase . . . . . I. FEM curve with 60-element mesh (Ref: 47) II. FEM curve with 128-element mesh III. Experimental	93

LIST OF TABLES

Table 1.	Yield Stress Values Obtained by Using 0.2% Offset Method . . . . .	76
----------	--	----

## I. INTRODUCTION

Many of the engineering materials used in practical applications are two-phase alloys. Alpha-beta brass, alpha-beta titanium, micro-duplex stainless steels, and copper-tin alloys are typical examples of such alloys that are of commercial and engineering importance. The mechanical properties of these materials are dependent on the characteristics of individual phases, the distribution and volume fraction of each phase, phase boundaries, and on grain boundaries. Mechanical properties are also affected by crystallography, strain-hardening, dislocation behavior, and slip systems in each of the phases.

Single-phase polycrystalline materials consist of individual grains that possess the same crystal structure and composition. In such single-phase materials, different regions with different crystallographic orientations are separated by grain boundaries. On the other hand, each phase in a two-phase material will possess different crystal structures and different chemical compositions. Because of their different compositions and crystal structures, the mechanical properties of the various phases will be different. Such two-phase materials will possess inter-phase boundaries in addition to grain boundaries.

To study the mechanical behavior of two-phase material, several models can be simulated. One of the models incorporates a phase boundary separating two single crystals

of individual phases formed by diffusion bonding (1). In another approach, a single crystal is joined to several large grains of another phase, so that there exists only one grain of this phase at the phase boundary in contact with the single crystal of the other phase (2). This model system is produced by melting the interface region, and is considered to produce a phase boundary that might correspond closer to those present in actual two-phase materials. A third model would comprise of duplex crystal (Widmanstätten platelets) with definite crystallographic orientation relationships between the two phases.

Studies on the mechanical properties of two-phase model systems have been conducted, in the past, by Hingwe et al. (2,3,4) and Nilsen et al. (5,6,7). They studied the room temperature mechanical properties of bicrystals of alpha-beta brass under uniaxial tension at various strain rates. Khezri-Yazdan et al. (8) conducted similar investigations at higher temperatures. Izumi et al. (9-15) have also studied mechanical properties of alpha-beta brass bicrystals produced by the diffusion bonding method. These studies on bicrystals of alpha-beta brasses have been aimed at understanding the basic deformation mechanisms of two-phase materials.

The engineering materials in use are polycrystalline, and to understand their mechanical behavior one needs to

study the deformation behavior of polycrystalline two-phase materials.

None of the above studies has dealt with the direct observations of detailed dislocation behavior in the phase boundary region. In the present investigation, the dislocation behavior in the phase boundary region of polycrystalline two-phase alpha-beta brass was studied by transmission electron microscopy. In addition, a finite element method (FEM) was used to study stress-strain behavior of alpha-beta brass.

study the deformation behavior of polycrystalline two-phase materials.

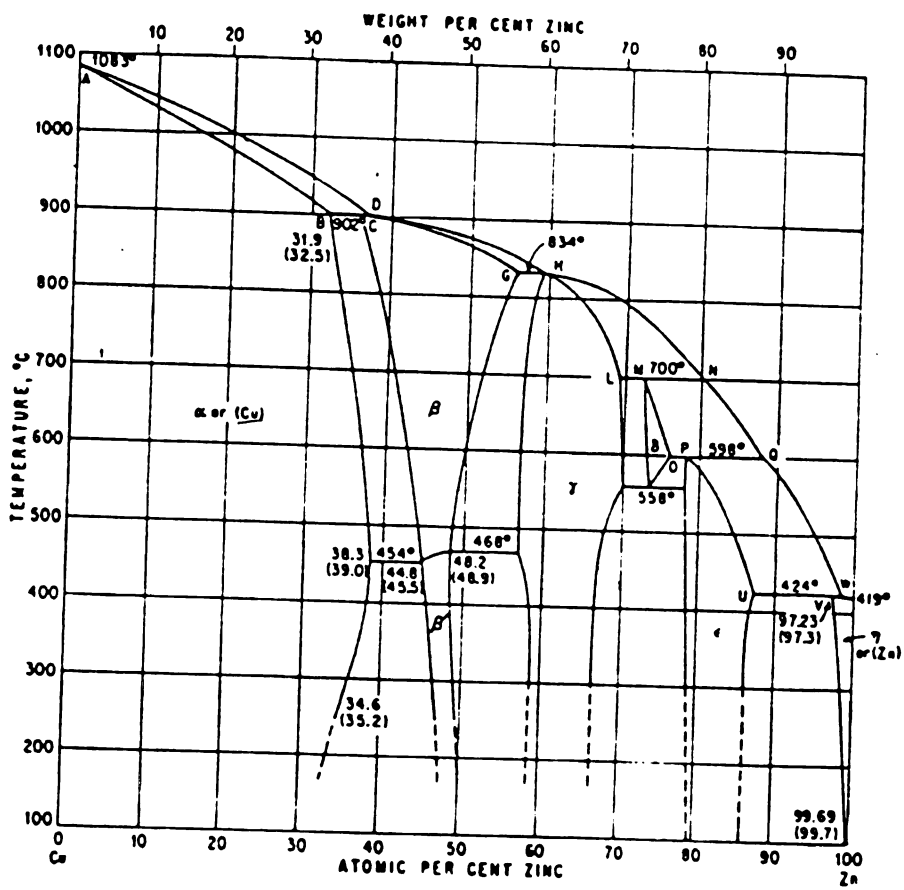
None of the above studies has dealt with the direct observations of detailed dislocation behavior in the phase boundary region. In the present investigation, the dislocation behavior in the phase boundary region of polycrystalline two-phase alpha-beta brass was studied by transmission electron microscopy. In addition, a finite element method (FEM) was used to study stress-strain behavior of alpha-beta brass.

## II. HISTORICAL BACKGROUND

### II-A. Copper-Zinc System

Brass is a class of commercial alloys which is comprised of copper and zinc with useful mechanical properties and corrosion resistance. A phase diagram of this system is presented in Figure 1. The alpha phase has a face-centered cubic (FCC) structure. This phase has a maximum solubility of about 38 weight percent zinc, as shown in this diagram. The alpha phase is fairly strong and possesses excellent ductility and formability. A secondary phase termed the beta phase forms above 38 weight percent zinc concentration. The beta phase has quite different properties as compared to the alpha phase. It has a cesium-chloride structure and is harder and stronger, but much less ductile than the alpha phase. Above approximately 454°C to 468°C (depending on composition), the beta phase has a disordered, body-centered cubic structure. In brasses with zinc composition of 38 to 46 weight percent, both alpha and beta phases are present. These brasses are known as alpha-beta brasses. Brass containing 40 weight percent of zinc and 60 weight percent of copper is representative of this class, and is known as "MUNTZ METAL." Muntz metal is used for the present investigation, so as to understand the role of an inter-phase boundary on the deformation behavior.

Figure 1. The copper-zinc phase diagram (Ref. 16).



## II-B. Deformation Behavior of Single Crystals of Alpha and Beta Brasses

Alpha brass single crystal has an FCC structure with zinc atoms occupying random positions in the copper lattice. Deformation of alpha brass occurs along close-packed {111} planes and along  $\langle 110 \rangle$  directions.

It has been suggested by Heidenreich and Shockley (17) that dislocations in FCC crystals, such as alpha brass, can split into two partial dislocations according to the reaction

$$\frac{a}{2} [110] = \frac{a}{6} [211] + \frac{a}{6} [12\bar{1}] ,$$

and thereby lower the energy of the system.

Alpha brass single crystals undergo three stages of work-hardening during uniaxial tensile deformation. The first stage is characterized by a low work-hardening rate which is influenced by crystal orientation, temperature, and purity. The second stage is characterized by a high work-hardening rate and is independent of crystal orientation and test variables. The third stage of hardening has a decreasing work-hardening rate due to dislocation climb and cross-slip of screw dislocations.

Ordered beta brass has cesium chloride (CsCl) structure below the critical temperature ( $T_c$ ). The CsCl structure is comprised of two interpenetrating simple cubes, one of copper atoms and the other of zinc, termed as B-2 type superlattice. This structure is illustrated in Figure 2.

Figure 2. Unit cell of ordered beta brass (A-Cu, B-Zn)  
(Ref. 19)

The slip system in the ordered beta structure is of  $\{110\}\langle T11 \rangle$  type. In B-2 type structures, when a dislocation, whose Burger's vector is a unit lattice vector, moves through an ordered lattice, there is a local rearrangement of atoms leading to the creation of an antiphase boundary. The high energy antiphase boundary can only be dissociated when another single unit dislocation passes through the plane of disorder. This pair of dislocations is termed as superlattice dislocation. Brown (18) has observed that a high stress is required for movement of such dislocations. Disordered beta brass exhibits a decreasing strain-hardening rate over its entire range of deformation. Orowan (20) has made observations on the factors influencing the strain-rate sensitivity of materials and has given the formula for strain rate ( $\dot{\epsilon}$ ) as,

$$\frac{d\epsilon}{dt} = \dot{\epsilon} = \rho b v ,$$

where  $\rho$  is dislocation density

$\dot{\epsilon}$  is strain rate

$b$  is Burger's vector of mobile dislocations

$v$  is average velocity of dislocations.

It was suggested by Johnson and Gilman (21) that the total strain is related to the density of mobile dislocations. It has been observed that the deformation of beta brass is highly strain-rate sensitive. With increasing strain rate, ease of movement of mobile dislocations decreases because of

the more frequent dislocation interactions. After the mobile dislocations are tangled, a higher stress is required to activate new dislocation sources. At this stage, rate of deformation corresponds to the rate of dislocation multiplication.

Titchener and Ferguson (22) investigated the dynamic compressive behavior of beta single crystals, and have observed upper and lower yield points. The upper and lower yield stresses were found to depend on both strain-rate and temperature. The yield stress increases significantly with increasing strain rate and with decreasing temperature. At strains greater than 4 percent, dynamically deformed material was found to be softer than that deformed statically. The dynamic work-hardening rate was less than the static work-hardening rate. Deformation bands were observed in Titchener and Ferguson's studies, although no twinning or jerky flow was apparent.

#### II-C. Deformation of Bicrystals of Alpha and Beta Brasses

Bicrystals of single-phase materials are comprised of two grains of same phase. Grain boundaries are an impediment for the motion of dislocations during plastic deformation of a bicrystal. When bicrystals are deformed, interaction of slip with the boundary occurs and sometimes slip propagates from one grain to another. A grain boundary is often referred to as a forest of dislocations.

McLean (23) studied some of the mechanical behaviors of grain boundaries in Cu-Zn alloys. The grain boundaries in alpha bicrystals have been observed to slide with respect to each other. A grain boundary with an orientation of  $45^\circ$  with respect to tensile axis was observed to undergo a continuous deformation, and necking took place at this grain boundary.

Chuang and Margolin (24) studied the stress-strain relationship of beta brass crystals. Three isoaxial bicrystals and one nonisoaxial bicrystal of beta brass, oriented to have the grain boundaries parallel to the axis of loading, were used in their studies to investigate the stress-strain relationships. It was found that grain boundary strengthening was greater in nonisoaxial bicrystals of beta brass.

#### II-D. Deformation Behavior of Polycrystals of Alpha and Beta Brasses

Deformation behavior in polycrystalline materials differ from that of a single crystal. The presence of grain boundaries impose added constraints when deformation of individual grains takes place. Grain boundaries have no repetitive pattern in their structures and hence it is difficult to clearly understand their deformation behavior.

Karashima (25,26) studied the deformation behavior of alpha brass polycrystals. He observed pile-up of dislocations against grain boundaries and sub-grain boundaries at low strains (1-5 percent). With increasing

1

degrees of deformation (5-10 percent), dislocations from two or three slip systems interacted and formed dislocation tangles and kinks. The dislocation sub-structure varied according to the degree of deformation and was correlated with work-hardening mechanisms in various stages. Work-hardening in the initial stages was mainly attributed to the back stresses caused by dislocations piling up against grain boundaries. Formation of Lomer-Cottrell sessile dislocations (27), and development of jogs due to interaction of dislocations with vacancies, become important as deformation progressed. A prominent feature in alpha brass is that most of the dislocations introduced during cold-working are confined to the primary slip planes (6). Karashima's (25, 26) studies on alpha brass showed that slip progresses through grain boundaries at above 8 percent strain with clear indications that slip was continuous across the boundary into the neighboring grain. This observation supports the view that some dislocations can apparently pass through the boundary (47) if adjacent grains possess favorable relative crystallographic orientations.

Greninger (28) has studied the plastic deformation of beta brass and found that parallel markings that appear on the surface of a crystal after slight deformation represent lattice transformation. The polished surface revealed two distinct structural characteristics:

- 1) fine hair-like lines referred to as slip bands, and
- 2) a relief which is corrugated.

Neither slip lines nor deformation bands were observed to continue through a grain boundary without changing direction, and both must have been related in some way to the beta lattice.

According to Head et al. (30),  $a[111]$ ,  $a[100]$ , and  $a/2[111]$  are types of dislocations that exist in the deformation structure of beta brass. Head et al. computed the theoretical image profiles of dislocations in beta brass using two-beam dynamical theory, and considering the full anisotropic strain fields of the dislocations. Comparing the theoretical and experimental images, it was concluded that the majority of dislocations in beta brass were screw dislocations of type  $\langle 111 \rangle$  gliding on  $\{110\}$ . Some of these  $\langle 111 \rangle$  dislocations split into two  $a/2\langle 111 \rangle$  dislocations. Other dislocations observed were of the  $\langle 010 \rangle$  type that were glissile on 001 .

#### II-E. Deformation of Two-Phase Materials

So far, this review has dealt with deformation of single-phase materials. A more complicated deformation behavior is observed in two-phase materials.

a) Deformation of Bicrystals of Two-Phase Materials: Different models such as bicrystal and duplex crystals have been used to understand the deformation of two-phase materials. Hingwe and Subramanian (3) deformed bicrystals

of alpha-beta brass in uniaxial tension to study the initiation of plastic deformation and its propagation across the phase boundary. Observations were made with the phase boundary perpendicular to the tensile axis. The effectiveness of the phase boundary as a barrier for slip propagation depends upon the relative crystallographic orientation of the two phases. This may be due to i) the difference in shear moduli of alpha and beta, ii) the difference in Burger's vector of slip dislocations in the two phases, and iii) the difference in the number of available slip systems.

Nilsen and Subramanian (6) carried out investigations on bicrystals of alpha-beta brass consisting of oriented and equiaxed duplex boundaries. Equiaxed boundaries were found to be more effective in blocking the propagation of deformation from alpha to beta phase than the oriented boundary. They concluded that wider slip bands formed in alpha phase produced more effective stress concentration so as to activate slip in beta phase across the boundary. Fine or multiple slip formed in alpha phase at high strain rates did not produce effective stress concentrations to cause slip across the phase boundary. High strain rates tend to form fine slip in alpha phase by activating many dislocation sources. Interaction of fine slip with the boundary caused multiple slip immobilizing a large fraction of the dislocations. Nilsen and Subramanian (5) have also carried



out tensile tests on bicrystals of alpha-beta brass at various strain-rates, and for specimens having two different types of boundary geometries, corrugated and flat. They found out that corrugated boundary was more effective in blocking the propagation of slip from alpha to beta phase. All specimens tested were found to be strain-rate sensitive. At low strain rates, both boundary types were found to be ineffective barriers to the propagation of slip, and coarse slip was observed in the alpha phase. At higher strain rates, fine slip was observed in alpha phase.

Slip propagation in the beta phase requires the movements and multiplication of superlattice dislocations. Motion of superlattice dislocation is difficult and requires a high stress. As any slip line crosses from the alpha phase into the beta phase, it will proceed only to a limited extent. This extent depends upon the level of stress concentration created in alpha phase near the phase boundary. The effect of this stress concentration in beta phase diminishes in direct proportion to the distance from the phase boundary. When slip line in beta reaches a position at which the stress concentration is insufficient to continue slip propagation, it will stop.

Khezri-Yazdan (8) investigated the role of phase boundary orientation relative to the tensile axis in bicrystals of alpha-beta brass. In such a geometry the phase boundary experiences both shear and normal stresses

under uniaxial loading. In bicrystals with inclined boundaries, the pile-up stress due to interaction of slip in the alpha phase with the phase boundary was not the motivating force for creating deformation in beta phase. In these specimens, slip in beta phase normally occurred on its own. This may be due to the shear stress acting on the inclined boundaries. Takasugi, Izumi and Fat-Halla (12-15) tested diffusion-bonded alpha-beta bicrystals at specific strain-rates at various temperatures. They studied the specimens with the phase boundary parallel to the tensile axis. Under such loading conditions, the strain in alpha and beta phases are the same, and the boundary does not experience any stress.

Interface studies by Takasugi and Izumi (11) on bicrystals of alpha-beta brass led them to believe that the phenomenon of interface sliding was strongly dependent on the nature of the interface; i.e., the crystallographic orientation relationship, shear direction, and microstructure of the interface. Izumi et al. (9) have studied operative slip systems in diffusion-bonded alpha-beta brass two-phase bicrystals at 150°K. They found out that the primary  $(111)_\alpha$   $[T01]_\alpha$  system, in the alpha phase, and the primary  $P_\beta$   $[111]_\beta$ , in the beta phase, were operative ( $P_\beta$  being the actual observed slip plane in the beta phase lying between  $[T01]$  and  $[\bar{1}\bar{1}2]$ ). H. Kawazoe et al. (10) have performed fatigue tests on diffusion-bonded two-phase

bicrystals of alpha-beta brass. Fatigue testing at room temperature was performed at 30 Hz in tension-compression under constant stress amplitude of about  $\pm 100$  MPa. Predominant slip in the alpha phase occurred on the primary (111) plane, while those in the beta phase occurred on the planes apart from the (T01) plane rather close to the ( $\bar{2}$ 11) plane.

b) Deformation of Polycrystals of Alpha-Beta Brass:

Honeycomb and Boas (31) conducted metallographic studies of deformed alpha-beta brass containing 40 percent zinc. Initial deformation started in alpha phase and after heavy deformation in alpha, slip was observed in beta grains. When deformed specimens of alpha-beta brass were repolished and strained further, slip lines were found to appear again in alpha grains. Slip traces occasionally crossed the alpha-beta phase boundaries and the grains that deformed had parallel slip traces. The orientation relationships required between the alpha and beta brass, for slip propagation through the boundary to occur, was  $\{110\}_\beta \parallel \{111\}_\alpha$  and  $\langle 111 \rangle_\beta \parallel \langle 110 \rangle_\alpha$ . Grains satisfying these orientation conditions are called contiguous grains. Substantial deformation in beta was observed in the vicinity of alpha-beta phase boundary more than in the interior of beta grains.

## II-F. Theoretical Models for Interaction of Slip with Boundaries

Grain boundaries are one of the most important barrier to dislocation motion during plastic deformation of polycrystalline solids. During plastic deformation, the dislocations tend to pile up at grain boundaries. Because of this pile-up, a back stress is created which eventually may stop the dislocation source from operating (7). When stress concentration at a grain boundary is high enough, slip proceeds across the boundary and moves into a coherent slip plane in the adjacent region (7).

Various theories have been proposed to explain the continuation of slip through the boundary into the adjacent grain. A proposition of Hall (32) and Petch (33) is that a dislocation pile-up can "burst" through a grain boundary due to stress concentrations at the head of the pile-up. If  $\tau_a$  is the applied resolved shear stress on the slip plane, then stress acting on the head of the pile-up containing "n" dislocations is  $(n\tau_a)$ . The number of dislocations in a pile-up depends on the length of the pile-up, which in turn, is proportional to the grain diameter. Cottrell (34) used a somewhat similar approach. He suggested that it is virtually impossible for dislocations to "burst" through boundaries. Instead, he assumed that the stress concentration produced by a pile-up in one grain can activate dislocation sources in the adjacent grain.

Li (36) has pointed out that grain boundary can be a source of dislocations. According to him, irregularities at a grain boundary (steps, or ledges) could be responsible for emission of dislocations into the adjacent grains. Li has suggested that the grain boundary ledges can generate dislocations, "pumping" them into the adjacent grain.

Murr (37), among others, has shown that the grain boundaries could actually emit dislocations. He observed the emission of dislocations from a grain boundary source. In his study, dislocations were observed to be generated at the grain boundary ledge. There have also been further evidences in transmission electron microscopic studies indicating that grain boundaries can be a source of dislocations (38). It is presently thought that dislocation emission from grain boundaries is an important source of dislocations in the early stages of plastic deformation of a polycrystal (35,37,38).

#### II-G. Finite Element Method

To conduct an investigation of the stress-strain response in alpha-beta brass, the finite element method (FEM) was adopted. FEM is a numerical technique used for solving various problems in stress analysis (39). With this technique, the stress distribution in individual phases and stress-strain behavior of two-phase region can be ascertained.

Fishmeister and Sundstrom (40) used the FEM technique to calculate the stress-strain curves for different hardness ratios between different phases present in plain carbon steels (0.11 and 0.21 weight percent carbon) and aluminum bronzes (8 to 12 percent aluminum). They also studied deformation of individual phase regions in case of plain carbon steel by using two-dimensional ("plate") model of the ferrite-martensite microstructure. Karlsson and Sundstrom (41) have also studied plastic deformation in ferritic-martensitic steels. They used FEM to study inhomogeneity in corresponding two-phase model. They found that strain field is very inhomogeneous in two-phase structure and inhomogeneity increases substantially with increasing yield stress ratio. Sundstrom (42) has used FEM to study the elastic-plastic behavior of WC-CO alloys. He showed that continuum mechanics can be applied to a two-dimensional model of real microstructure. His results indicated that the plastic strain distribution calculated using FEM is very inhomogeneous on the microscale, and that FEM cannot give a high resolution on the microscale of stress and strain fields in the phases. This is because of computational limitations leading to coarser sub-division of the model into elements. Jinoch et al. (39) used FEM to study stress-strain curves of an alpha-beta Ti-8Mn alloy. In their investigation, they used a uniform mesh of 392 triangular two-dimensional (plane stress) plate elements. The volume

fraction, particle size, and shape could be varied by designating each triangle as either alpha or beta. The shapes of the particle used in the meshes were not the same as those in actual specimens but were idealized to make calculations simpler while maintaining the volume fraction constant at 17 percent. Their studies showed that an FEM-calculated stress-strain curve attained lower stress levels for similar strain levels as compared to an experimentally calculated stress-strain curve. This difference may be due to the finer grain sizes in the Ti-8Mn alloy and the contribution of the interface phase, which were not considered. Margolin et al. (43,44) studied the influence of particle size, matrix, and volume fraction of the phases on the stress-strain relationship of alpha-beta Ti alloys. They found that for a given volume fraction of second phase, the calculated stress-strain curve was higher for specimens with a finer particle size as compared to that of specimens with coarser particle size. For the stronger beta phase, the stress-strain curve reached higher stress values. There were discrepancies between the experimental values and calculated values in general, because the anisotropy of alpha and beta phase was not considered and no distinctions were made between the slip behavior for equiaxed and Widmanstätten alpha. It was also observed that average strain in alpha phase was higher than average strain in beta phase. Maximum strain in alpha occurred at the center of

the alpha particle, away from the constraints imposed by beta. On the other hand, maximum strain in beta phase occurred at the alpha-beta interface, because of the need for beta to maintain compatibility with the alpha particle.

### III. EXPERIMENTAL PROCEDURE

#### III-A. Procedures Used for Transmission Electron Microscopic Study of the Deformation Structure in the Phase Boundary Region

Stock of Muntz metal (60 percent Cu, 40 percent Zn) was rolled down to a thickness of about 0.45 to 0.50 millimeters using a cold rolling mill. Tensile samples with a gauge length of 18 millimeters and a width of 7 millimeters were cut out. These samples were annealed for one hour at 425°C in evacuated quartz tubes to relieve prior stresses in the material. These specimens were then imparted a critical strain of 8 percent plastic strain and heat-treated for 18 hours at 825°C in evacuated quartz tubes to obtain large grain sizes. These heat-treated samples were strained to 12-27 percent plastic strains at 0.2 cm/min strain rate. A microtensile fixture fitted onto an Instron testing machine was used to strain the samples. These deformed specimens were thinned down chemically to 0.10 millimeters using 45 percent nitric acid and 55 percent distilled water solution and washed with methanol. A disc of 3 millimeters' diameter was cut out of the gauge length of the specimen. Two-step polishing techniques were used to produce electron transparent regions. It is difficult to thin samples so as to have transparent areas at the interface region consisting of both alpha and beta phases, owing to the possibility of selective polishing of one of the two phases and etching of the phase boundary (45). Although several conditions and

chemicals have been tried, the best results were obtained using the following conditions and electrolyte.

Jet polishing was carried out to achieve a concave surface on one side of the sample using the set-up shown in Figure 3. Conditions and chemicals used were as follows:

Electrolyte: 12 volume percent nitric acid, 88 percent methyl alcohol

Voltage: 60 volts (DC)

Temperature: 243°K

Time: 2 minutes.

Final polishing was used to obtain a small hole at the center of the specimen. This hole was produced by using a cylindrical cathode immersed in the electrolyte mentioned below. The specimen was held between two platinum loops as shown in Figure 4. A light source was used to detect the hole as soon as it was formed. Subsequently, the specimen was washed thoroughly with methanol.

Electrolyte: 12 volume percent nitric acid, 88 percent methyl alcohol

Voltage: 7.5 volts (DC)

Temperature: 243°K

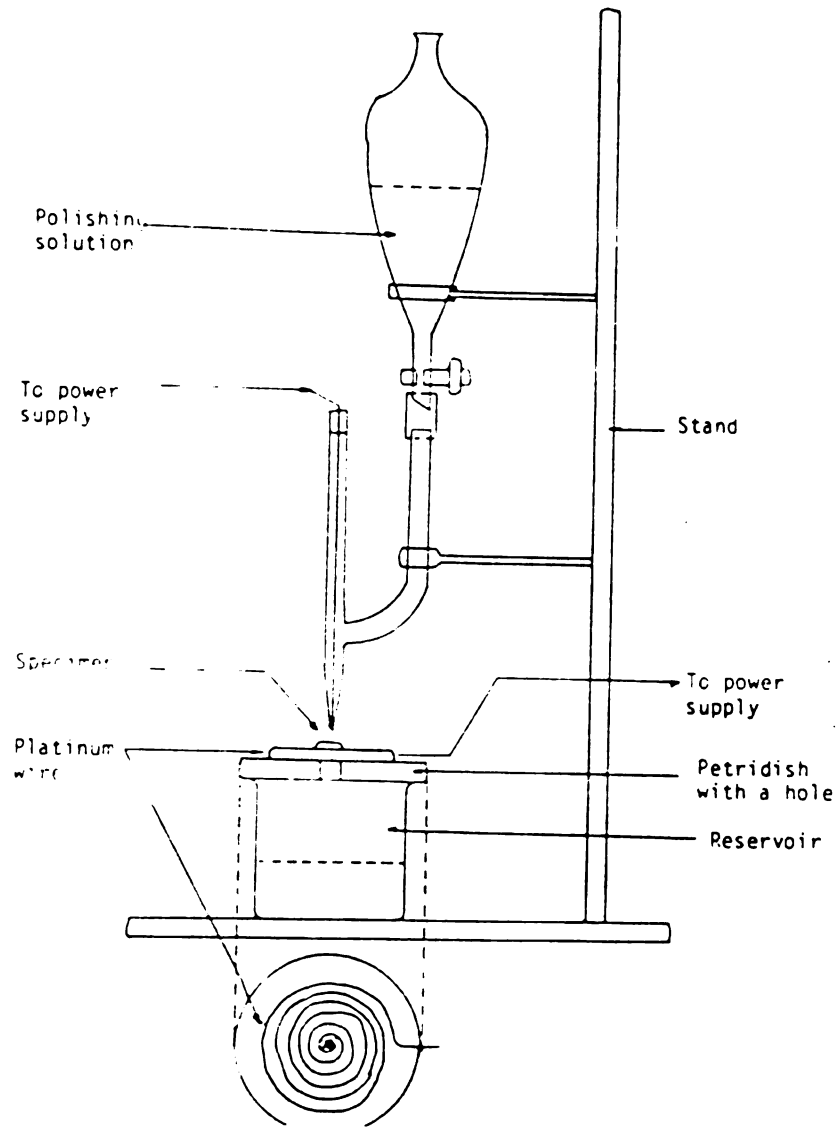
Time: 1-2 minutes.

These specimens were observed in an EM-300 Transmission Electron Microscope operated at 100 Kv.



Figure 3. Schematic of "jet-polishing" unit (by courtesy of S. Shekhar, MMM, Michigan State University).

esy of





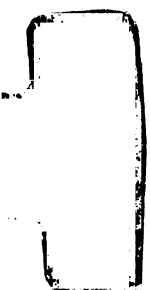
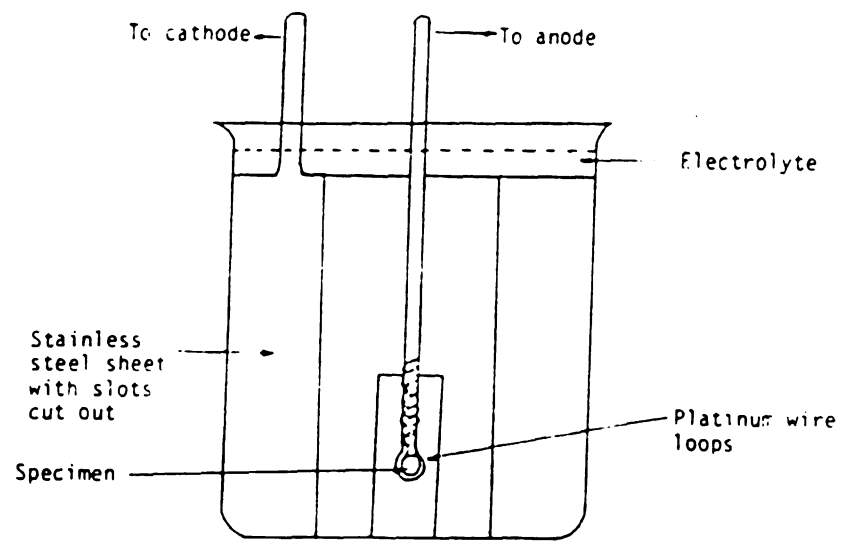


Figure 4. Schematic of the final electropolishing unit (by courtesy of S. Shekhar, MMM, Michigan State University).

unit (by  
te



### III-B Finite Element Analysis

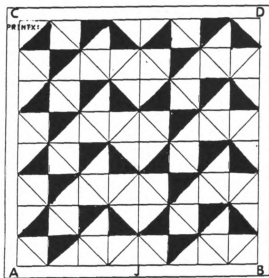
FEM analysis was carried out using a Prime 750 computer system analysis computer program, which is used for the solution of several classes of engineering problems and which was utilized for the present study. The ANSYS Element Library (46) offers 95 different element types to carry out a wide range of engineering analyses. Element type STIF (42) was used for analysis of alpha-beta brass. In order to generate a nonlinear stress-strain relationship, the Young's modulus, Poisson's ratio, and five strains in the nonlinear region of the stress-strain curve with corresponding stress have to be defined (46). A mesh of 128 elements was prepared for the ANSYS, and FEM analysis was carried out with various volume percent of beta phase and grain sizes. In a prior study, Kulkarni (47) used a mesh of 60 elements for FEM analysis. Dividing the area into more number of elements increases the degree of accuracy; hence, a 128-element mesh was prepared for this analysis. Comparison of the results obtained by using these two different meshes is presented in detail in the next section.

Node "J" was fixed in the meshes shown in Figures 5, 6 and 7, and all other nodes along AB could move in both X- and Y-directions. Node along  $\overline{CD}$  had the same "Y" displacement. Input stress-strain curves used are shown in Figure 8. The stress-strain curve for alpha brass was based on the stress-strain curve of brass containing 70 weight

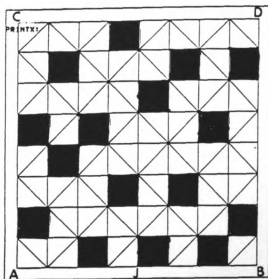


Figure 5. FEM mesh for alpha-beta brass containing 25 volume percent beta phase (beta phase is shaded dark):

- A) Fine grain distribution.
- B) Medium grain distribution.



A

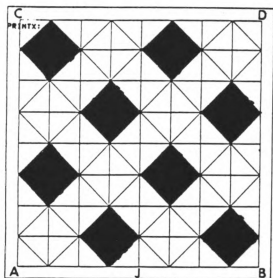


B



Figure 5 (continued)

C) Coarse grain distribution.



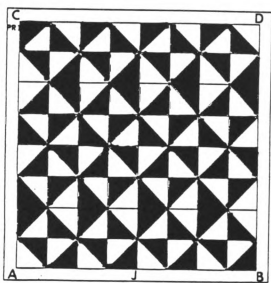
C



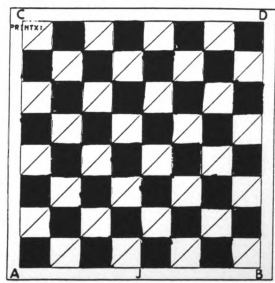
Figure 6. FEM mesh for alpha-beta brass containing 50 volume percent beta phase (beta phase is shaded dark):

- A) Fine grain distribution.
- B) Medium grain distribution.

aded



A

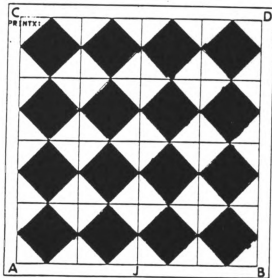


B



Figure 6 (continued)

C) Coarse grain distribution.

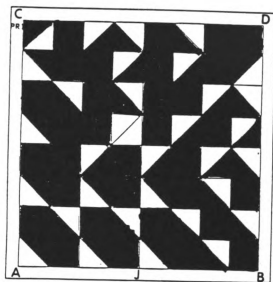


C

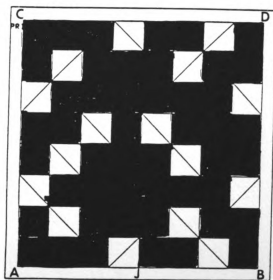


Figure 7. FEM mesh for alpha-beta brass containing 75 volume percent beta phase (beta phase is shaded dark):

- A) Fine grain distribution.
- B) Medium grain distribution.



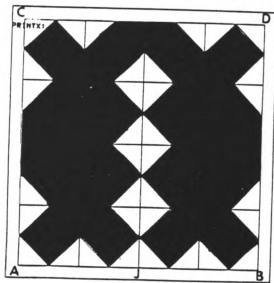
A



B

Figure 7 (continued)

C) Coarse grain distribution.



C

11

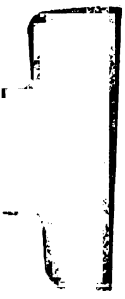
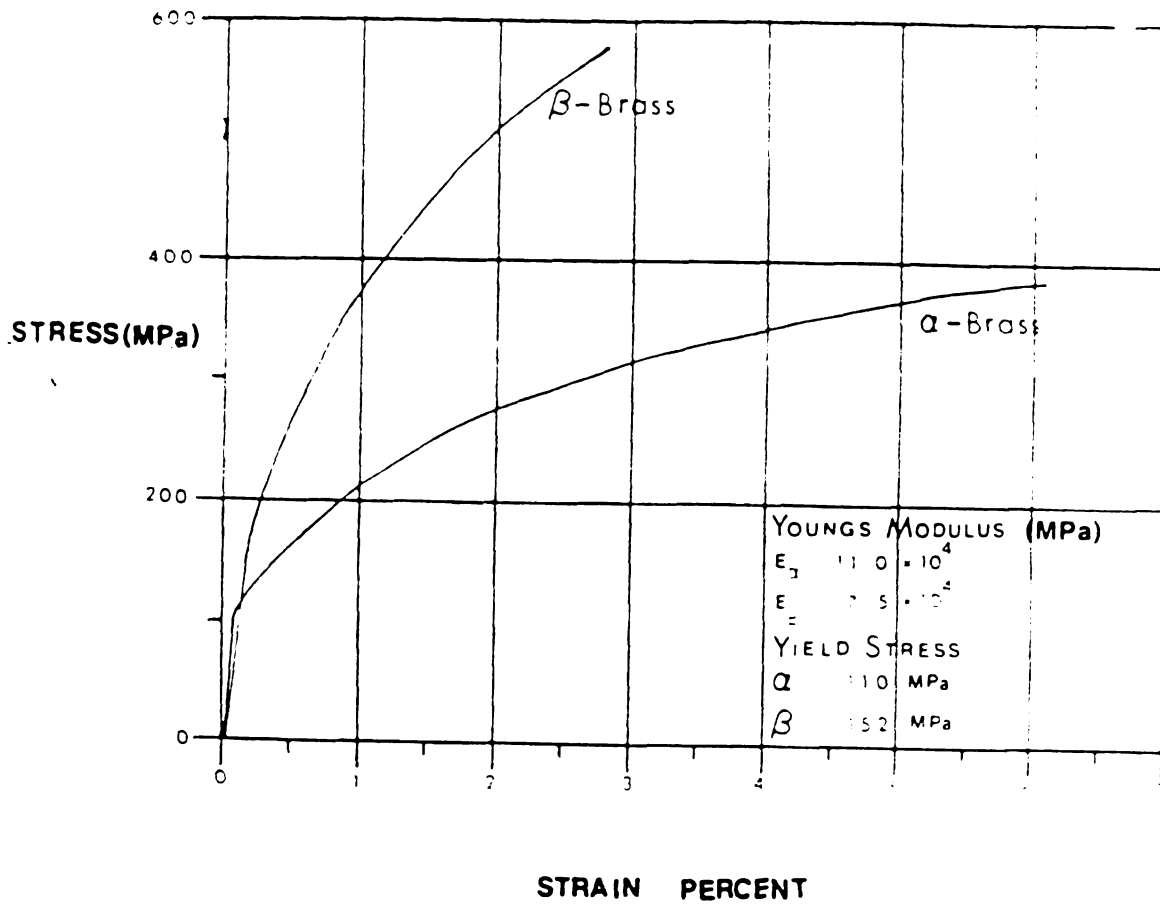


Figure 8. FEM input stress-strain curve of Alpha and Beta brasses (Ref. 48).

1 Beta



percent copper and 30 weight percent zinc. The stress-strain curve for beta brass was obtained from the available values of Young's modulus, yield stress, and the corresponding strain value at the yield stress level (48). To obtain the stress-strain curves, the applied stresses were known for each loading condition. The corresponding strains were calculated from the common displacements of the nodes on the line  $\overline{CD}$  and the initial length  $\overline{AC}$ . Stress-strain distribution plots were obtained by using the mesh shown in Figure 9. Stresses at neighboring triangular elements were averaged to deduce stress at the center of each square on line  $\overline{GG}$ . Displacement in the "Y"-direction of two successive nodes were used for calculation of strains.

Stress-strain curves were plotted for the two-phase region (alpha, beta) for two different loading configurations. In the first case tensile axis was normal to the phase boundary, and in the second case tensile axis was parallel to the phase boundary. The above two cases are illustrated in Figure 10. Similarly, stress-strain curves were plotted for 25, 50, and 75 volume percent of beta phase. For each volume percent of beta phase, three different grain sizes were analyzed.

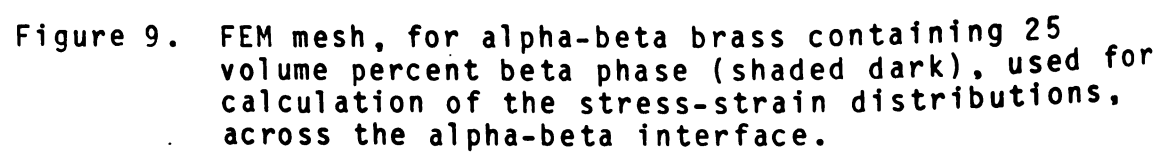
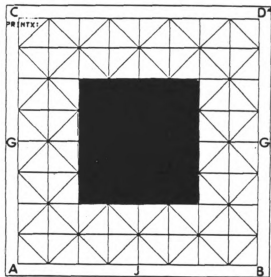
The figure, which is missing from the page, would depict a finite element mesh for a material with two phases. One phase, the alpha phase, would be represented by a lighter mesh, and the other phase, the beta phase, which constitutes 25% of the volume, would be represented by a darker mesh. The mesh would be used to analyze the stress and strain at the interface between these two phases.

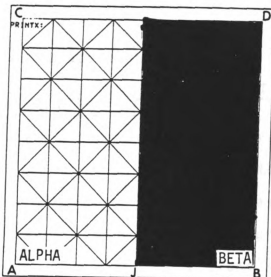
Figure 9. FEM mesh, for alpha-beta brass containing 25 volume percent beta phase (shaded dark), used for calculation of the stress-strain distributions, across the alpha-beta interface.

for  
5.

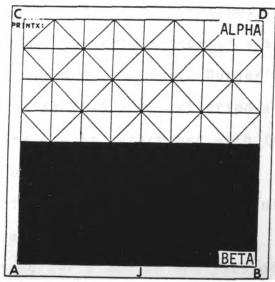


- 
- Figure 10. FEM mesh for alpha-beta brass containing 50 volume percent beta and 50 volume percent alpha.
- A) Phase boundary parallel to tensile axis.
  - B) Phase boundary perpendicular to tensile axis.

50  
alpha.  
s.  
e



A



B

## IV. RESULTS AND DISCUSSION

### IV-A. TRANSMISSION ELECTRON MICROSCOPE ANALYSIS OF THE DEFORMATION STRUCTURE IN ALPHA-BETA BRASS

This study is divided into the following parts:

- a) Burger's vector analysis of dislocations present near grain and phase boundaries, and
  - b) analysis of interaction of dislocations with equiaxed phase boundary.
- a) ANALYSIS OF DISLOCATIONS PRESENT NEAR GRAIN AND PHASE BOUNDARIES

This study mainly focused on the Burger's vector analysis of the dislocations present in the deformation structure of the two-phase alpha-beta brass near a) alpha-alpha grain boundary, and b) alpha-beta phase boundary. Burger's vector analysis of dislocations near the boundary was performed to determine the character of dislocations. Two parameters are needed in the dislocation analysis to determine the character of dislocations. These two parameters are the Burger's vector of dislocation and the orientation of dislocation line. Burger's vector can be determined by using " $\vec{g} \cdot \vec{b} = 0$ " criterion and orientation of dislocation line can be determined with the help of stereographic projection.

A total of eight analyses are presented in this thesis. They are divided as follows:

- i) Three Burger's vector analyses of dislocations present near alpha-alpha grain boundary,

## IV. RESULTS AND DISCUSSION

### IV-A. TRANSMISSION ELECTRON MICROSCOPE ANALYSIS OF THE DEFORMATION STRUCTURE IN ALPHA-BETA BRASS

This study is divided into the following parts:

- a) Burger's vector analysis of dislocations present near grain and phase boundaries, and
- b) analysis of interaction of dislocations with equiaxed phase boundary.

#### a) ANALYSIS OF DISLOCATIONS PRESENT NEAR GRAIN AND PHASE BOUNDARIES

This study mainly focused on the Burger's vector analysis of the dislocations present in the deformation structure of the two-phase alpha-beta brass near a) alpha-alpha grain boundary, and b) alpha-beta phase boundary. Burger's vector analysis of dislocations near the boundary was performed to determine the character of dislocations. Two parameters are needed in the dislocation analysis to determine the character of dislocations. These two parameters are the Burger's vector of dislocation and the orientation of dislocation line. Burger's vector can be determined by using " $\vec{g} \cdot \vec{b} = 0$ " criterion and orientation of dislocation line can be determined with the help of stereographic projection.

A total of eight analyses are presented in this thesis. They are divided as follows:

- i) Three Burger's vector analyses of dislocations present near alpha-alpha grain boundary,

ii) Four Burger's vector analyses of dislocations present in alpha region near alpha-beta phase boundary, and

iii) one Burger's vector analysis of dislocations present in beta region near alpha-beta phase boundary.

In all these tables, " $\theta$ " represents the angle between the Burger's vector and the dislocation line direction.

i) Burger's Vector Analyses of Dislocations Present Near (Alpha-Alpha) Grain Boundary (#1-#3)

Analysis #1

Dislocations which are present in slip traces marked "a" and "b" in Figure 11 were analyzed. A set of five micrographs with three different  $\vec{g}$  vectors was obtained with different tilting conditions. Possible Burger's vector of these dislocations can be determined by using the following table where "X" represents cases for which the " $\vec{g} \cdot \vec{b} = 0$  criterion" is satisfied and "-" represents cases for which the " $\vec{g} \cdot \vec{b} = 0$  criterion" is not satisfied.

Figure Number	$\vec{g}$	Possible Burger's Vector					
		[110]	[1T0]	[101]	[10T]	[011]	[01T]
11A, B	$[\bar{2}00]$	-	-	-	-	X	X
11C, D	$[2\bar{2}0]$	X	-	-	-	-	-
11E	$[0\bar{2}0]$	-	-	X	X	-	-

Dislocation trace analysis was carried out as shown in the following table:

Figure 11. Dislocations near grain boundary in alpha phase of alpha-beta brass specimen deformed to 12 percent strain level.

A)  $\vec{g} = [\bar{2}00]$ .

(110)



A

11

Figure 11 (continued)

B)  $\vec{g} = [200]$ .

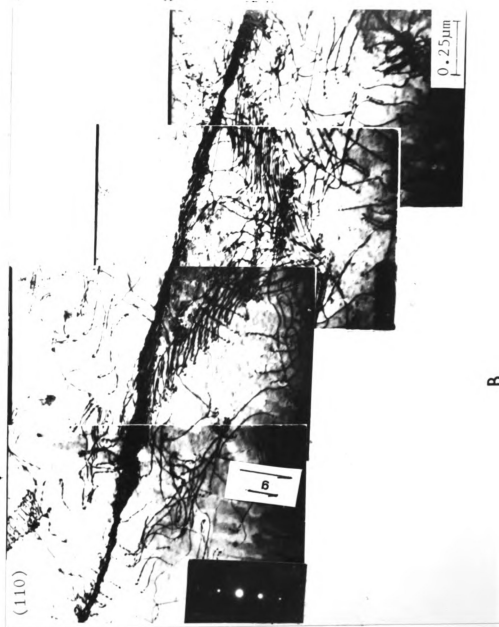


Figure 11 (continued)

c)  $\vec{g} = [2\bar{2}0]$ .

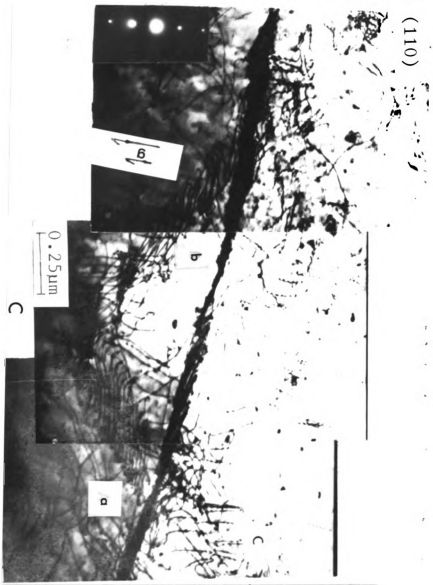


Figure 11 (continued)

D)  $\vec{g} = [2\bar{2}0]$ .

(110)

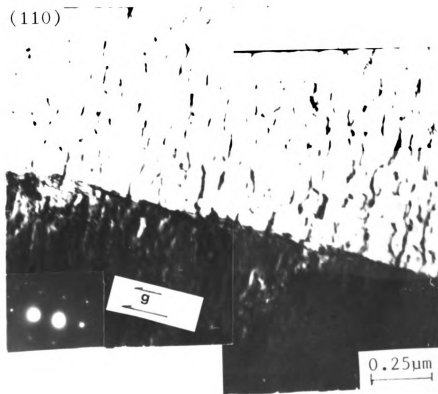


D

Figure 11 (continued)

$$E) \vec{g} = [0\bar{2}0].$$

(110)



E

Dislocations Present in Slip Traces	Burger's Vector	Slip Plane	Dislocation Line Direction	Dislocation Character
a	[101]	(11 $\bar{1}$ ) ( $\bar{1}$ 11) N•P	[011]	Mixed $\theta = 60^\circ-85^\circ$
	[10 $\bar{1}$ ]	(111) [1 $\bar{1}$ 1] N•P	[0 $\bar{1}$ 1]	Mixed $\theta = 120^\circ-145^\circ$
	[1 $\bar{1}$ 0]	(111) (11 $\bar{1}$ )	[0 $\bar{1}$ 1]	Mixed $\theta = 60^\circ-85^\circ$
			[011]	Mixed $\theta = 120^\circ-145^\circ$
b	[101]	(11 $\bar{1}$ ) N•P ( $\bar{1}$ 11)	[0 $\bar{1}$ 1]	Mixed $\theta = 60^\circ-80^\circ$
	[10 $\bar{1}$ ]	(111) N•P (1 $\bar{1}$ 1)	[011]	Mixed $\theta = 120^\circ-140^\circ$

N•P in the above table represents that the particular slip plane is not a possible one.

### Analysis #2

Dislocations present in slip trace "a" in Figure 12 were analyzed. A set of four micrographs was obtained with different tilting conditions. Possible Burger's vector can be determined from the following table:

1

figu

Figure 12. Dislocations near grain boundary in alpha phase of alpha-beta brass. Location of grain boundary: upper right corner  $60^\circ$  to X-axis.

A)  $\vec{g} = [1\bar{1}1]$ .

B)  $\vec{g} = [\bar{1}\bar{3}1]$ .

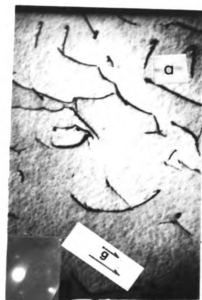
C)  $\vec{g} = [\bar{2}\bar{2}0]$ .

D)  $\vec{g} = [0\bar{4}2]$ .

Specimen deformed to 12 percent strain level.



A



B



C



D

Figure Number	$\vec{g}$	Possible Burger's Vector					
		[110]	[1T0]	[101]	[10T]	[011]	[01T]
12A	[1T1]	X	-	-	X	X	-
12B	[T31]	-	-	X	-	-	-
12C	[220]	-	X	-	-	-	-
12D	[042]	-	-	-	-	-	-

Dislocation trace analysis was carried out as shown below:

Dislocations Present in Slip Traces	Burger's Vector	Slip Plane	Dislocation Line Direction	Dislocation Character
a	[01T]	(111) (T11) N.P	[0T1]	Screw

### Analysis #3

Dislocations present in slip trace marked "a" in Figure 13 were analyzed. A set of three micrographs was obtained with different tilting conditions. Possible Burger's vector of these dislocations can be determined from the following table:

Figure 13. Dislocations near grain boundary in alpha phase of alpha-beta brass. Specimen deformed to 12 percent strain level.

A)  $\vec{g} = [T1T]$ .

B)  $\vec{g} = [00\bar{2}]$ .

C)  $\vec{g} = [T11]$ .



A



B



C

Figure Number	$\vec{g}$	Possible Burger's Vector					
		[110]	[1T0]	[101]	[10T]	[011]	[01T]
13A	[T1T]	X	-	-	X	X	-
13B	[00Z]	X	X	-	-	-	-
13C	[T11]	X	-	X	-	-	X

Dislocation trace analysis was carried out as shown below:

Dislocations Present in Slip Traces	Burger's Vector	Slip Plane	Dislocation Line Direction	Dislocation Character
a	[1T0]	(111)	[T10]	Screw
		(11T)	[T10]	Screw

ii) Burger's Vector Analyses of Dislocations Present in Alpha Region Near Alpha-Beta Phase Boundary (#4-#7)

Analysis #4

Dislocations present in slip traces marked "a," "b," and "c" in Figure 14 were analyzed. A set of three micrographs was obtained with different tilting conditions. Possible Burger's vector of these dislocations can be determined from the following table:

Figure Number	$\vec{g}$	Possible Burger's Vector					
		[110]	[1T0]	[101]	[10T]	[011]	[01T]
13A	[T1T]	X	-	-	X	X	-
13B	[00Z]	X	X	-	-	-	-
13C	[T11]	X	-	X	-	-	X

Dislocation trace analysis was carried out as shown below:

Dislocations Present in Slip Traces	Burger's Vector	Slip Plane	Dislocation Line Direction	Dislocation Character
a	[1T0]	(111)	[T10]	Screw
		(11T)	[T10]	Screw

ii) Burger's Vector Analyses of Dislocations Present in Alpha Region Near Alpha-Beta Phase Boundary (#4-#7)

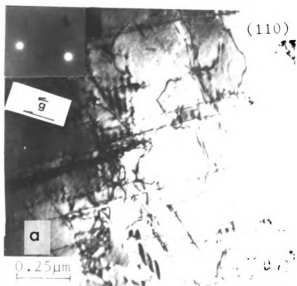
Analysis #4

Dislocations present in slip traces marked "a," "b," and "c" in Figure 14 were analyzed. A set of three micrographs was obtained with different tilting conditions. Possible Burger's vector of these dislocations can be determined from the following table:

Figure 14. Dislocations in alpha region near alpha-beta phase boundary. Specimen deformed to 12 percent strain level. Location of phase boundary: lower left corner  $50^\circ$  to X-axis.

A)  $\vec{g} = [00\bar{2}]$ .

B)  $\vec{g} = [\bar{1}11]$ .



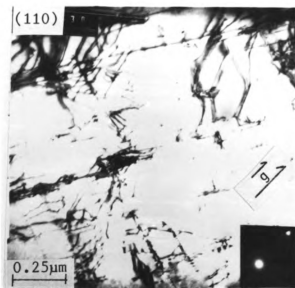
A



B

Figure 14 (continued)

c)  $\vec{g} = [1\bar{1}1]$ .



C

Figure Number	$\vec{g}$	Possible Burger's Vector					
		[110]	[1T0]	[101]	[10T]	[011]	[01T]
14A	[00Z]	X	X	-	-	-	-
14B	[T11]	X	-	X	-	-	X
14C	[1T1]	X	-	-	X	X	-

Dislocation trace analysis was carried as shown below:

Dislocations Present in Slip Traces	Burger's Vector	Slip Plane	Dislocation Line Direction	Dislocation Character
a	[101]	(11T) N•P (T11)	[1T2]	Mixed $\theta = 30^\circ-45^\circ$
	[01T]	(111) N•P (T11)	[1T2]	Mixed $\theta = 150^\circ-165^\circ$
b	[1T0]	(111) (11T)	[01T] [101]	Mixed $\theta = 120^\circ-155^\circ$ Mixed $\theta = 60^\circ-95^\circ$
	c	[10T]	(111) N•P (1T1)	[1T2]
[011]		(11T) N•P (1T1)	[1T2]	Mixed $\theta = 150^\circ-170^\circ$

Analysis #5

Dislocations present in the slip trace marked "a," "b" and "c" in Figure 15 were analyzed. A set of three micrographs was obtained with different tilting conditions. Possible Burger's vectors of these dislocations can be determined from the following table:

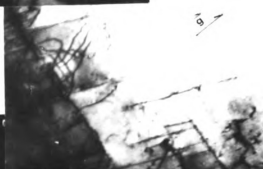
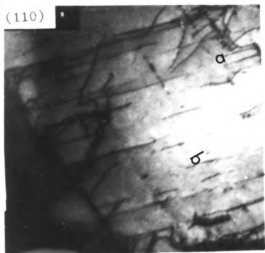
Figure Number	$\vec{g}$	Possible Burger's Vector					
		[110]	[1T0]	[101]	[10T]	[011]	[01T]
15A	[1T1]	X	-	-	X	X	-
15B	[T11]	X	-	X	-	-	X
15C	[00 $\bar{2}$ ]	X	X	-	-	-	-

Dislocation trace analysis was carried out as shown on page 56:

Figure 15. Dislocations in alpha region near alpha-beta phase boundary. Specimen deformed to 15 percent strain level.

A)  $\vec{g} = [1\bar{1}1]$ .

(110)



A

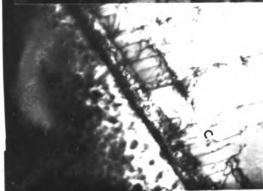
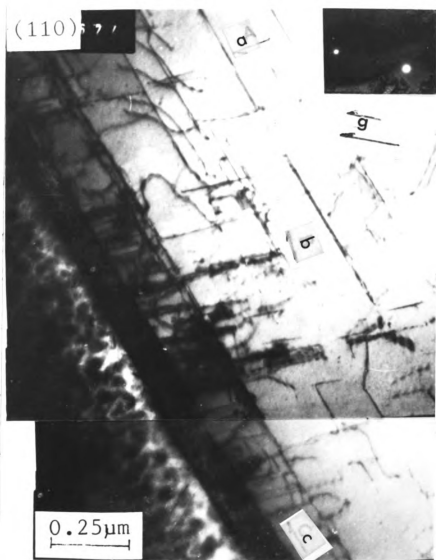


Figure 15 (continued)

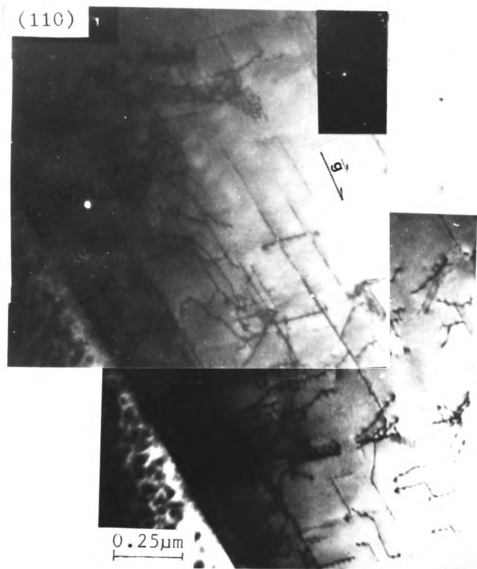
B)  $\vec{g} = [\bar{1}11]$ .



**B**

Figure 15 (continued)

c)  $\vec{g} = [00\bar{2}]$ .



Dislocations Present in Slip Traces	Burger's Vector	Slip Plane	Dislocation Line Direction	Dislocation Character
a	[10T]	(111) N•P (1T1)	[1T2]	Mixed $\theta = 30^\circ-55^\circ$
	[011]	(11T) N•P (1T1)	[1T2]	Mixed $\theta = 150^\circ-175^\circ$
b	[101]	(T11) (11T) N•P	[1T2]	Mixed $\theta = 30^\circ-45^\circ$
	[01T]	(111) N•P (T11)	[1T2]	Mixed $\theta = 150^\circ-165^\circ$
c	[101]	(T11) N•P (11T)	[101]	Screw
	[01T]	(111) (11T) N•P	[01T]	Screw

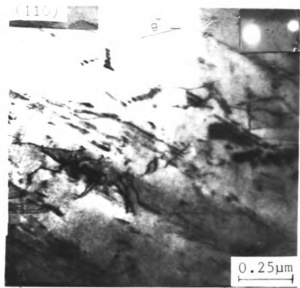
### Analysis #6

Dislocations present in the slip traces marked "a," and "b" in Figure 16 were analyzed. A set of three micrographs was obtained with different tilting conditions. Possible Burger's vector of these dislocations can be determined from the following table:

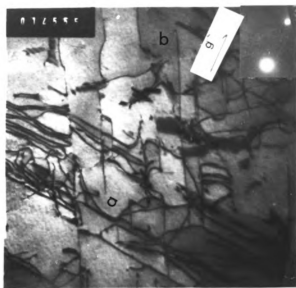
Figure 16. Dislocations in alpha region near alpha-beta phase boundary. Specimen deformed to 15 percent strain level. Location of phase boundary: vertical, left.

A)  $\bar{g} = [\bar{1}11]$ .

B)  $\bar{g} = [002]$ .



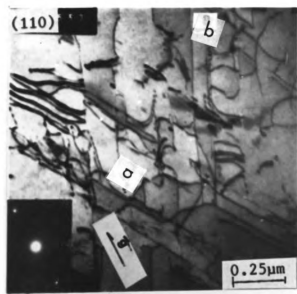
A



B

Figure 16 (continued)

$$c) \vec{g} = [1\bar{1}1].$$



C

Figure Number	$\vec{g}$	Possible Burger's Vector					
		[110]	[1T0]	[101]	[10T]	[011]	[01T]
16B	[002]	X	X	-	-	-	-
16A	[T11]	X	-	X	-	-	X
16C	[1T1]	X	-	-	X	X	-

Dislocation trace analysis was carried out as shown below:

Dislocations Present in Slip Traces	Burger's Vector	Slip Plane	Dislocation Line Direction	Dislocation Character	
a	[101]	(11T)	[1T0]	Mixed	
	(T11) N•P			$\theta = 60^\circ - 100^\circ$	
	[01T]	(111)	[1T0]	Mixed	
b	[101]	(T11) N•P		$\theta = 120^\circ - 160^\circ$	
		(T11)	[101]	Screw	
	[01T]	(111) N•P			
		(T11)	[101]	Mixed	$\theta = 120^\circ - 135^\circ$

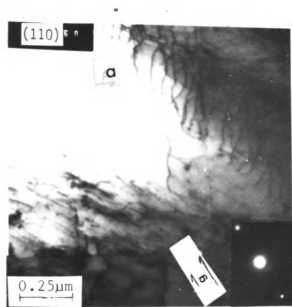
### Analysis #7

Dislocations present in slip trace marked "a" in Figure 17 were analyzed. A set of three micrographs was obtained

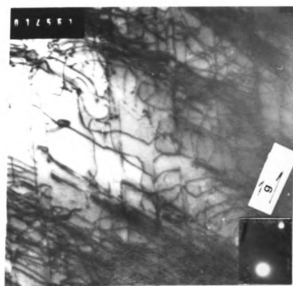
Figure 17. Dislocation in alpha region near alpha-beta phase boundary. Specimen deformed to 18 percent strain level. Location of phase boundary: vertical, left.

A)  $\bar{g} = [1\bar{1}1]$ .

B)  $\bar{g} = [002]$ .



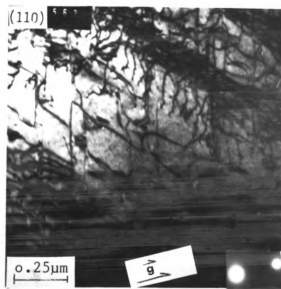
A



B

Figure 17 (continued)

c)  $\vec{g} = [T11]$ .



C

with different tilting conditions. Possible Burger's vectors of these dislocations can be determined from the following table:

Figure Number	$\vec{g}$	Possible Burger's Vector					
		[110]	[1T0]	[101]	[10T]	[011]	[01T]
17A	[1T1]	X	-	-	X	X	-
17B	[002]	X	X	-	-	-	-
17C	[T11]	X	-	X	-	-	X

Dislocation trace analysis was carried out as shown below.

Dislocations Present in Slip Traces	Burger's Vector	Slip Plane	Dislocation Line Direction	Dislocation Character
a	[1T0]	(111)	[01T]	Mixed $\theta = 120^\circ - 170^\circ$
		(11T)	[101]	Mixed $\theta = 60^\circ - 110^\circ$

iii) Burger's Vector Analysis of Dislocations Present in  
Beta Region Near Alpha-Beta Phase Boundary (#8)

Analysis #8

Dislocations present in slip trace marked "a" in Figure 18 were analyzed. A set of four micrographs was obtained with different tilting conditions. Possible Burger's vector of these dislocations can be determined from the following table:

Figure Number	$\vec{g}$	Possible Burger's Vector			
		[111]	[111]	[1T1]	[11T]
18A	[200]	-	-	-	-
18B	[110]	-	X	X	-
18C	$[\bar{1}\bar{2}\bar{1}]$	-	X	-	X
18D	[T10]	X	-	-	X

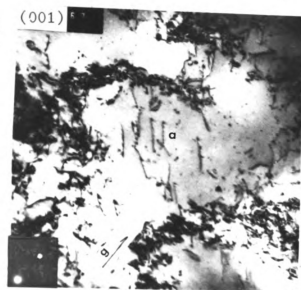
Dislocation trace analysis was carried out as shown below:

Dislocations Present in Slip Traces	Burger's Vector	Slip Plane	Dislocation Line Direction	Dislocation Character
a	[111]	(1T0)	[111]	Screw
		(10T)	[111]	Screw
		(01T) N•P		

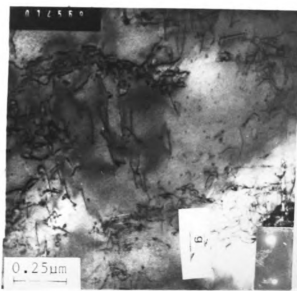
Figure 18. Dislocations in beta region near alpha-beta phase boundary. Specimen strained to 18 percent strain level. Location of phase boundary: lower left corner,  $65^\circ$  to X-axis.

A)  $\vec{g} = [\bar{2}00]$ .

B)  $\vec{g} = [110]$ .



A

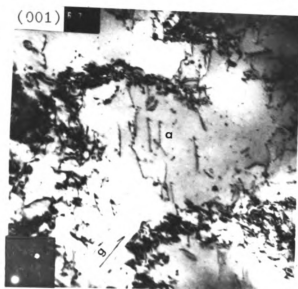


B

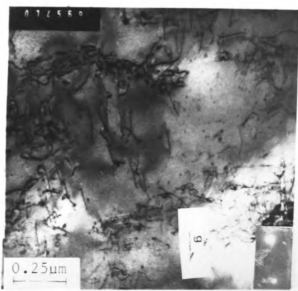
Figure 18. Dislocations in beta region near alpha-beta phase boundary. Specimen strained to 18 percent strain level. Location of phase boundary: lower left corner,  $65^\circ$  to X-axis.

A)  $\vec{g} = [\bar{2}00]$ .

B)  $\vec{g} = [110]$ .



A

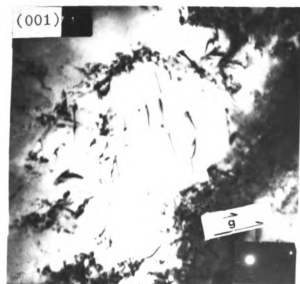


B

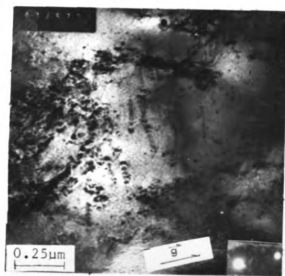
Figure 18 (continued)

C)  $\vec{g} = [\bar{1}\bar{2}\bar{1}]$ .

D)  $\vec{g} = [\bar{1}10]$ .



C



D

Individual dislocations present in beta phase were observed at regions away from the phase boundary. These slip dislocations were screw in character and of the type  $\frac{a}{2}\langle 111 \rangle$  gliding on  $\{T10\}$ . Such an observation is consistent with studies of Head et al. (30).

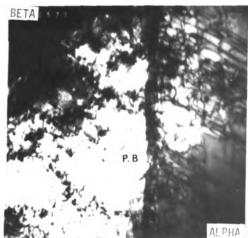
b) INTERACTION OF DISLOCATIONS WITH EQUIAXED PHASE BOUNDARY

The micrographs which are presented in Figure 19 reveal dislocation pile-up at the equiaxed phase boundary in alpha region, and some slip dislocations in beta region. Three models have been proposed to explain the initiation of deformation in the adjacent grain due to interaction of slip in one grain with the boundary. According to Hall (32) and Petch (33) a dislocation pile-up can "burst" through a boundary due to stress concentration at the head of the pile-up. Cottrell (34) suggested that the stress concentration produced by a pile-up in one grain can activate dislocation sources in the adjacent grain. According to Li (36), stress concentration created due to the pile-up at the boundary forces the boundary dislocation sources into the adjacent grain. According to Nabarro (34), a slip band cannot cross from one grain to another without irregularity unless slip direction is the same in both the grains and the choice of the crystal plane for slip is not critical in the adjoining grain. Which one of the above models is applicable to alpha-beta phase boundary cannot be verified during the present study since dislocation pile-up

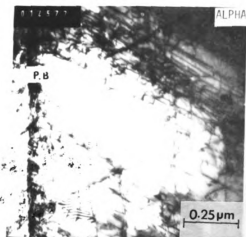
Figure 19. Deformation structure near phase boundary of alpha-beta brass.

A and B: Specimen deformed to 12 percent strain level.

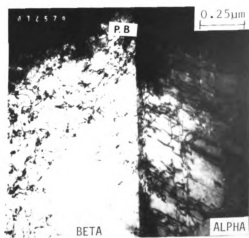
C and D: Specimen deformed to 15 percent strain level.



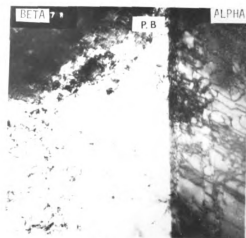
A



B



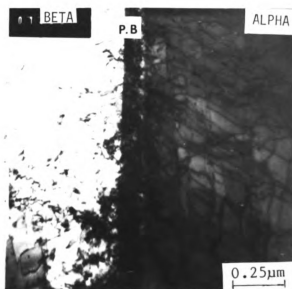
C



D

Figure 19 (continued)

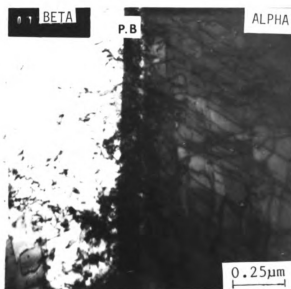
E) Specimen deformed to 18 percent strain level.



E

Figure 19 (continued)

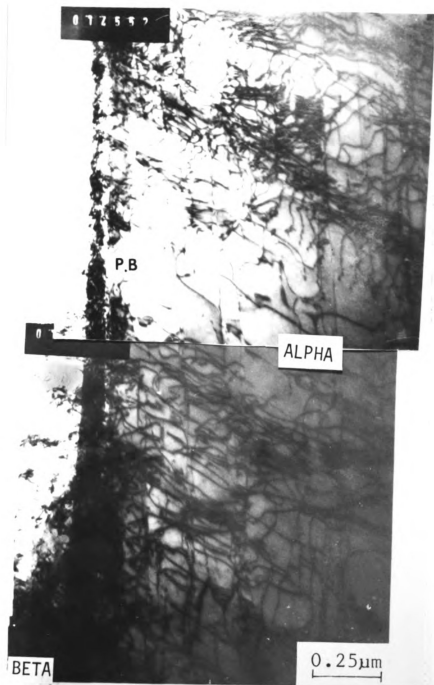
E) Specimen deformed to 18 percent strain level.



E

Figure 19 (continued)

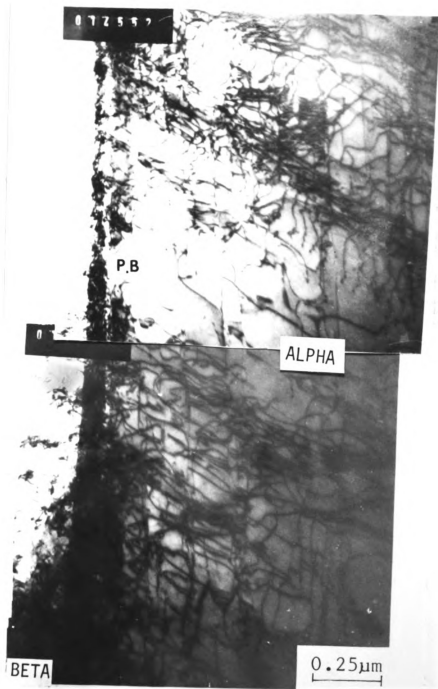
F) Specimen deformed to 20 percent strain level.



F

Figure 19 (continued)

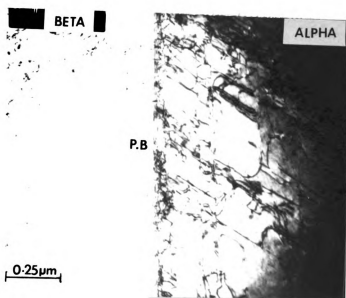
F) Specimen deformed to 20 percent strain level.



F

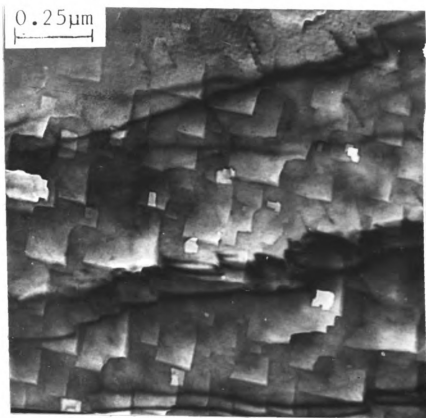
Figure 19 (continued)

G) Specimen deformed to 27 percent strain level.



G

Figure 20. Antiphase boundaries in beta region of alpha-beta brass.



in alpha at an equiaxed boundary never initiated slip in beta near the phase boundary in the range of strain levels studied.

In this study, the dislocation pile-ups in alpha region were observed at the phase boundary for specimens that were deformed to strain levels of more than 12 percent. This observation is consistent with the results of Karashima (25) and Kulkarni (47). Karashima observed complex tangled dislocation structures in 70 Cu-30 Zn alpha brass at strain levels higher than 5 percent. Similar observations were made by Kulkarni (47) in alpha phase of 60 Cu-40 Zn brass. Since beta brass has higher yield stress than alpha brass, plastic deformation starts earlier in alpha phase than in beta phase. At strain levels of 12 to 27 percent, the alpha phase exhibits dislocation pile-up at the phase boundary. There is no evidence of dislocation activity in beta phase near alpha-beta phase boundary as a result of this pile-up. A probable reason is that the adjacent alpha and beta grains did not possess the specific orientation relationship as has been mentioned by Honeycombe and Boas (31). They have stated that such slip propagation from alpha to beta can occur when both the grains are contiguous. Slip planes and slip directions in both phases will match with each other under such conditions.

There are other reasons for not observing dislocation activity in beta near the phase boundary. According to

Khezri-Yazdan (8), the pile-up stress in the alpha phase is not the motivating force for creating deformation in beta phase when phase boundary is inclined to tensile axis. Under such conditions, slip in beta phase normally occurs on its own. This may be due to the shear stresses acting on the inclined boundaries due to applied tensile loading.

In two-phase bicrystal studies with the phase boundary oriented either parallel or perpendicular to the tensile axis (2-6,9-15), the special constraints imposed by the loading geometry may facilitate activation of slip in beta phase as a result of dislocation pile-up in the alpha region at the boundary. Such constraints will be absent during deformation of polycrystals.

In the present study, slip initiation in beta as a result of dislocation pile-up in alpha did not occur. This may be due to the absence of specific relative crystallographic orientations of alpha and beta, and due to the presence of shear stresses (inclined boundary) in the phase boundary due to applied tensile loading.

#### IV-B. FEM ANALYSIS OF STRESS-STRAIN BEHAVIOR OF ALPHA-BETA BRASS

The result of present FEM analysis is divided as follows:

- a) Stress-strain relationship for alpha-beta brass containing 25, 50, and 75 volume percent of beta phase.

- b) Stress-strain relationship for small, medium, and coarse grain sizes of alpha and beta phases.
- c) Stress-strain distribution across alpha-beta interface.
- d) Stress-strain curve for two-phase region.
- e) Comparison of experimental and FEM calculated stress-strain curves.
- a) Stress-Strain Relationship for Alpha-Beta Brass Containing 25, 50, and 75 Volume Percent of Beta Phase

The FEM-calculated stress-strain curves for alpha-beta brass containing 25, 50, and 75 volume percent of beta phase are presented in Figure 21. It can be observed that the stress level increases with increasing beta volume for identical strain levels. Phase distribution and grain sizes used for calculation are shown in Figures 5A, 6A, and 7A. Yield stress values are determined using 0.2 percent offset method. These yield stress values are tabulated in Table 1.

- b) Stress-Strain Relationship for Small, Medium, and Coarse Grain Sizes of Alpha and Beta Phases

Stress-strain curves of alpha-beta brass with two different grain sizes are presented in Figures 22, 23, and 24 for 25, 50, and 75 volume percent of beta phase respectively. It can be seen from the figures that as the grain size gets smaller, a stress-strain curve tends to shift upwards; i.e., for equal strain levels, the stress-strain curve for finer grain size attains higher stress values than the stress-strain curve for a coarser grain

- b) Stress-strain relationship for small, medium, and coarse grain sizes of alpha and beta phases.
- c) Stress-strain distribution across alpha-beta interface.
- d) Stress-strain curve for two-phase region.
- e) Comparison of experimental and FEM calculated stress-strain curves.
- a) Stress-Strain Relationship for Alpha-Beta Brass Containing 25, 50, and 75 Volume Percent of Beta Phase

The FEM-calculated stress-strain curves for alpha-beta brass containing 25, 50, and 75 volume percent of beta phase are presented in Figure 21. It can be observed that the stress level increases with increasing beta volume for identical strain levels. Phase distribution and grain sizes used for calculation are shown in Figures 5A, 6A, and 7A. Yield stress values are determined using 0.2 percent offset method. These yield stress values are tabulated in Table 1.

- b) Stress-Strain Relationship for Small, Medium, and Coarse Grain Sizes of Alpha and Beta Phases

Stress-strain curves of alpha-beta brass with two different grain sizes are presented in Figures 22, 23, and 24 for 25, 50, and 75 volume percent of beta phase respectively. It can be seen from the figures that as the grain size gets smaller, a stress-strain curve tends to shift upwards; i.e., for equal strain levels, the stress-strain curve for finer grain size attains higher stress values than the stress-strain curve for a coarser grain

Figure 21. FEM-calculated stress-strain curves for alpha-beta brass containing 25, 50, and 75 volume percent of beta phase. Grain size: small.

- I. %  $V_{\beta}$  - 25%.
- II. %  $V_{\beta}$  - 50%.
- III. %  $V_{\beta}$  - 75%.

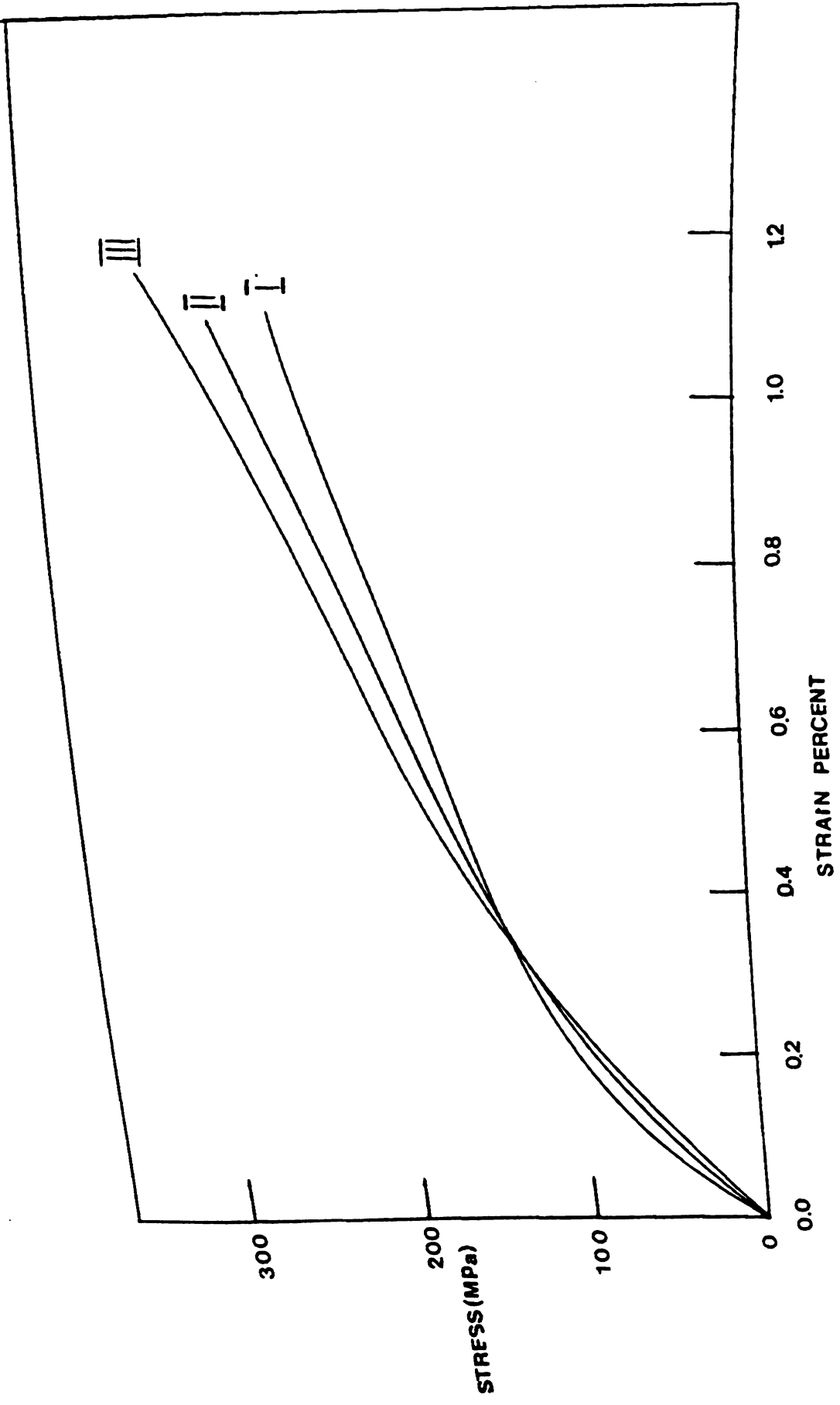


Table 1

Yield Stress Values Obtained by Using 0.2% Offset Method

Curve	Volume Percent Beta Phase	Yield Stress (MPa)
I	25	180
II	50	205
III	75	240

Figure 22. FEM-calculated stress-strain curves of alpha-beta brass containing 25 volume percent beta phase for fine (I) and coarse (II) grain size distribution.

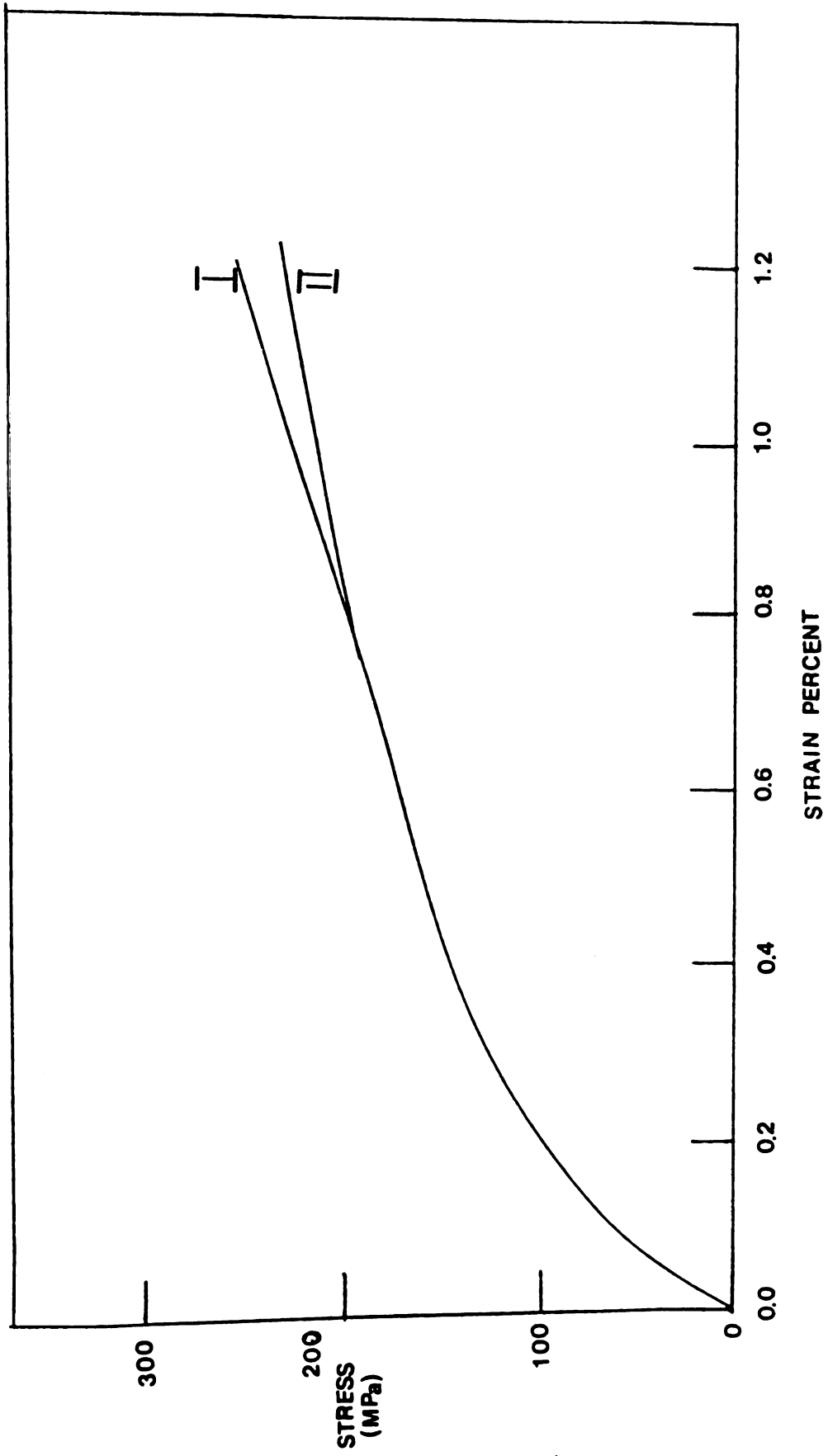


Figure 22. FEM-calculated stress-strain curves of alpha-beta brass containing 25 volume percent beta phase for fine (I) and coarse (II) grain size distribution.

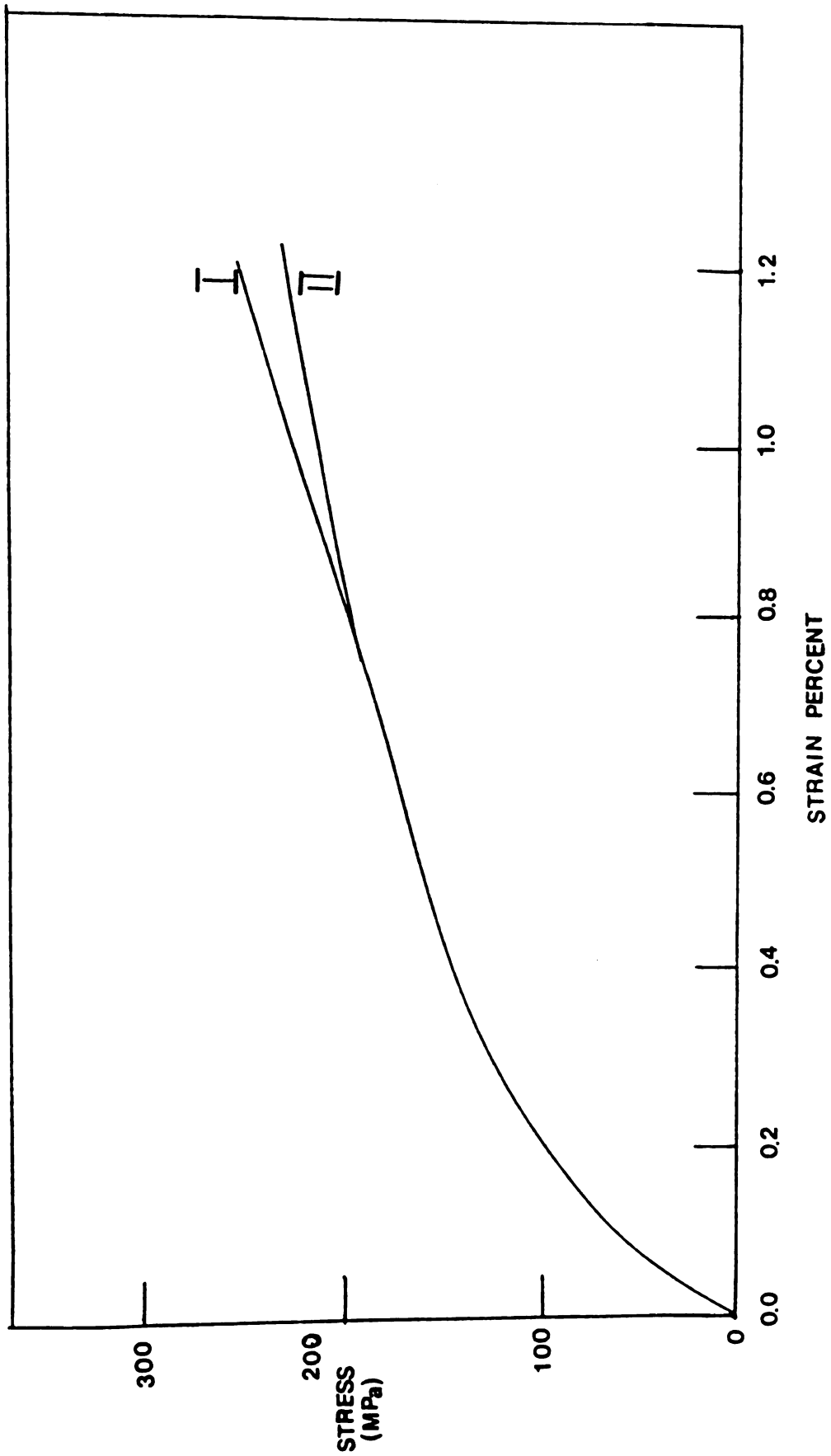


Figure 23. FEM-calculated stress-strain curves of alpha-beta brass containing 50 volume percent beta phase for fine (I) and coarse (II) grain size distribution.

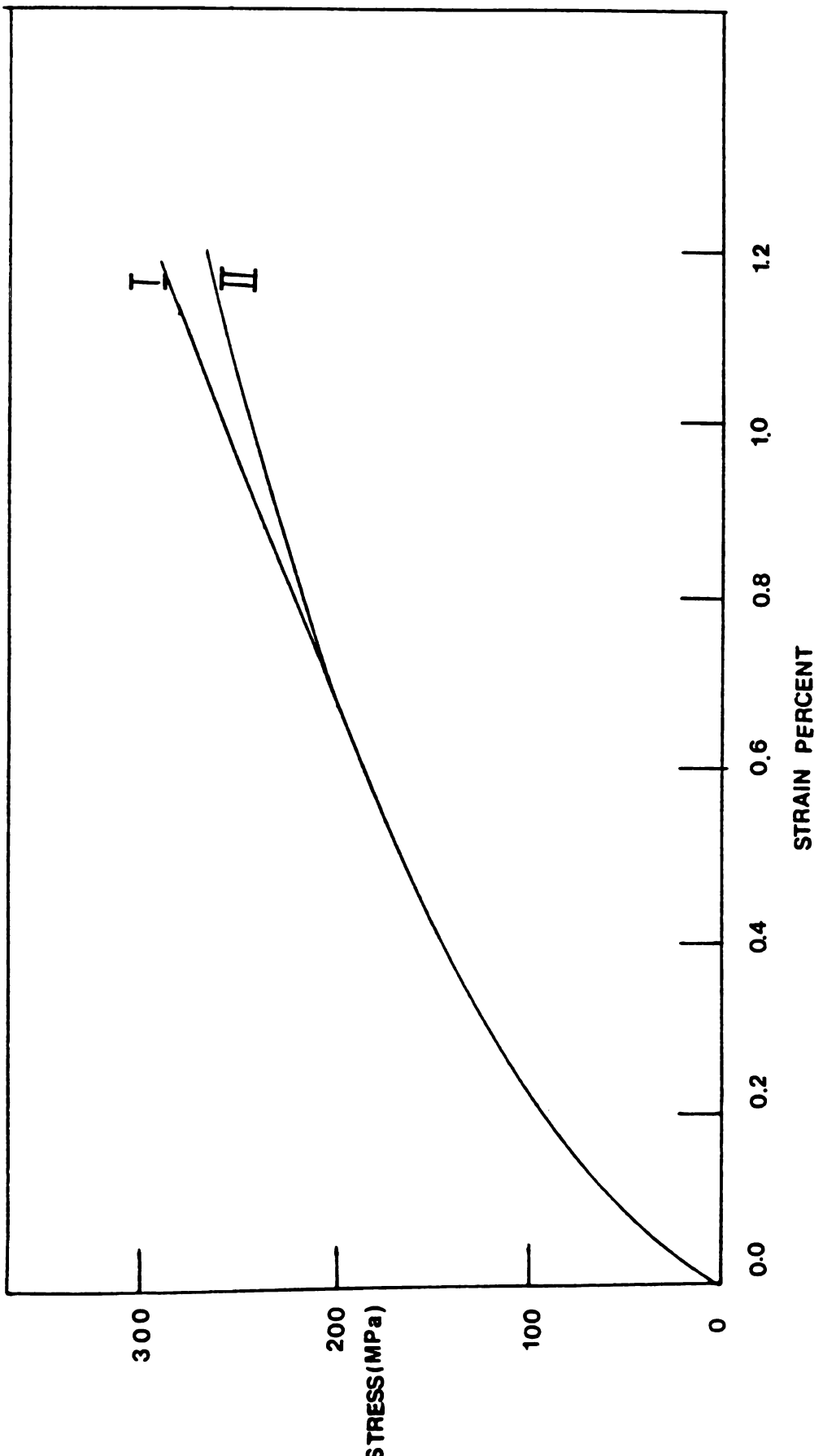
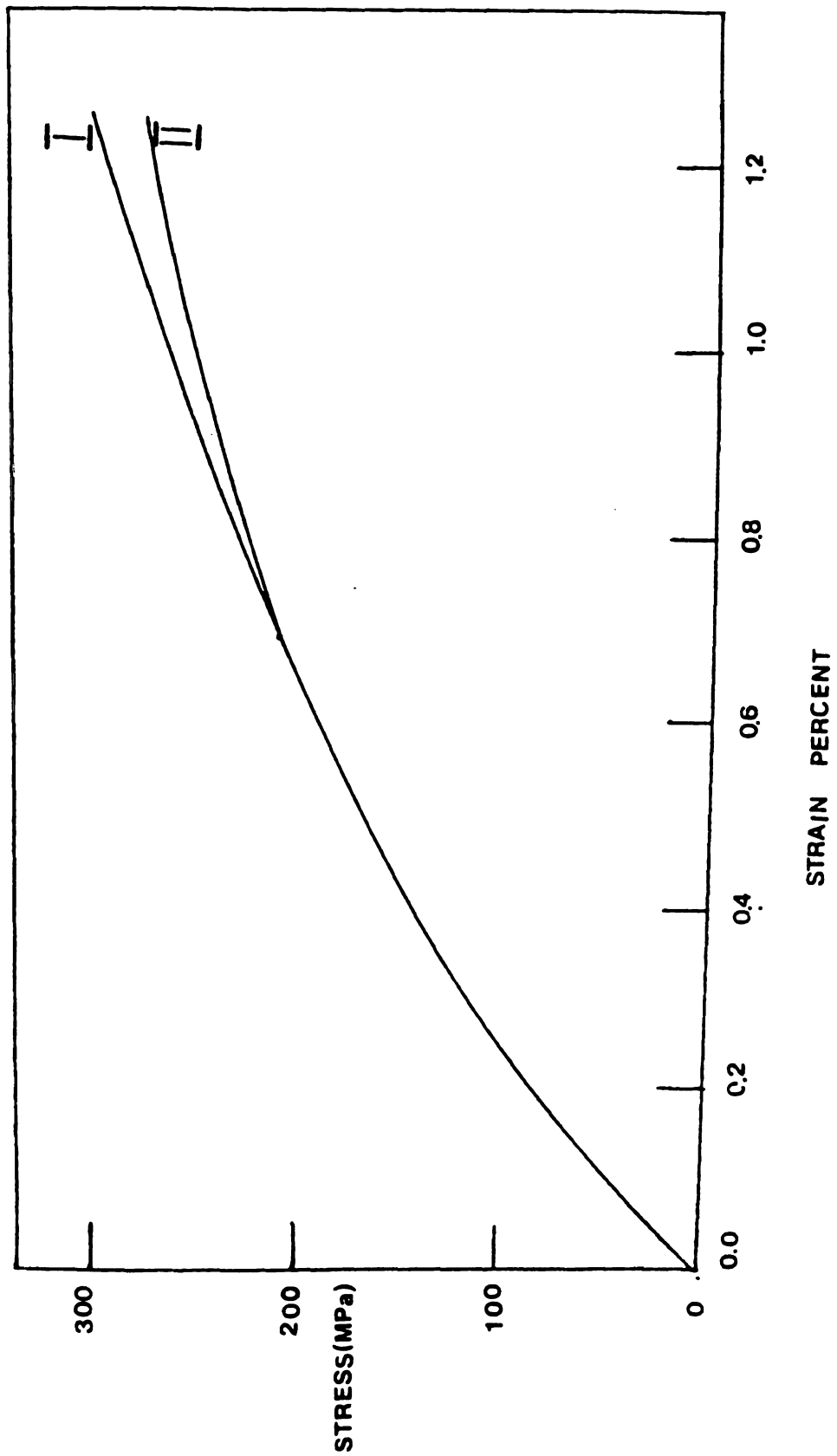


Figure 24. FEM-calculated stress-strain curves of alpha-beta brass containing 75 volume percent beta phase for fine (I) and coarse (II) grain size distribution.



size. According to Jinoch et al. (39), flow stress, at a given strain level, for a finer particle size is higher than for a coarser particle size. This is because the strain difference between alpha and beta phase is smaller for a finer particle size (39). For a finer particle size the difference in strain levels between alpha and beta phases is not significant, whereas for coarser particle size the difference in strain is quite significant. As a result, the stiffer beta phase undergoes greater strain which in turn induces the stress levels to reach higher values. Thus the stress-strain curve for specimen with a fine particle size reaches higher stress levels than the curve for specimen with coarse particle size.

c) Stress-Strain Distribution Across Alpha-Beta Interface

Stress distribution across the alpha-beta interface are plotted in Figures 25 and 26. It is calculated along loading "Y" direction and transverse "X" direction. The distribution of stress has been evaluated for stress levels of 172, 207, and 241 MPa for distribution in "Y" and "X" directions. The stresses in beta phases are higher than in stresses in alpha phases for any given external applied stress. Stress distribution in transverse "X" direction also showed steep gradient across the phase boundary.

Strain distribution across the phases is presented in Figure 27. Strains in beta phases were higher than in alpha at any given stress level. Stress and strain distributions

Figure 25. FEM-calculated stress distribution plot in alpha and beta region of alpha-beta brass containing 25 volume percent beta phase in the Y-direction ( $\sigma_{yy}$ )

Applied stress level:

▲ 172 MPa

● 207 MPa

X 241 MPa

Grain size: small.

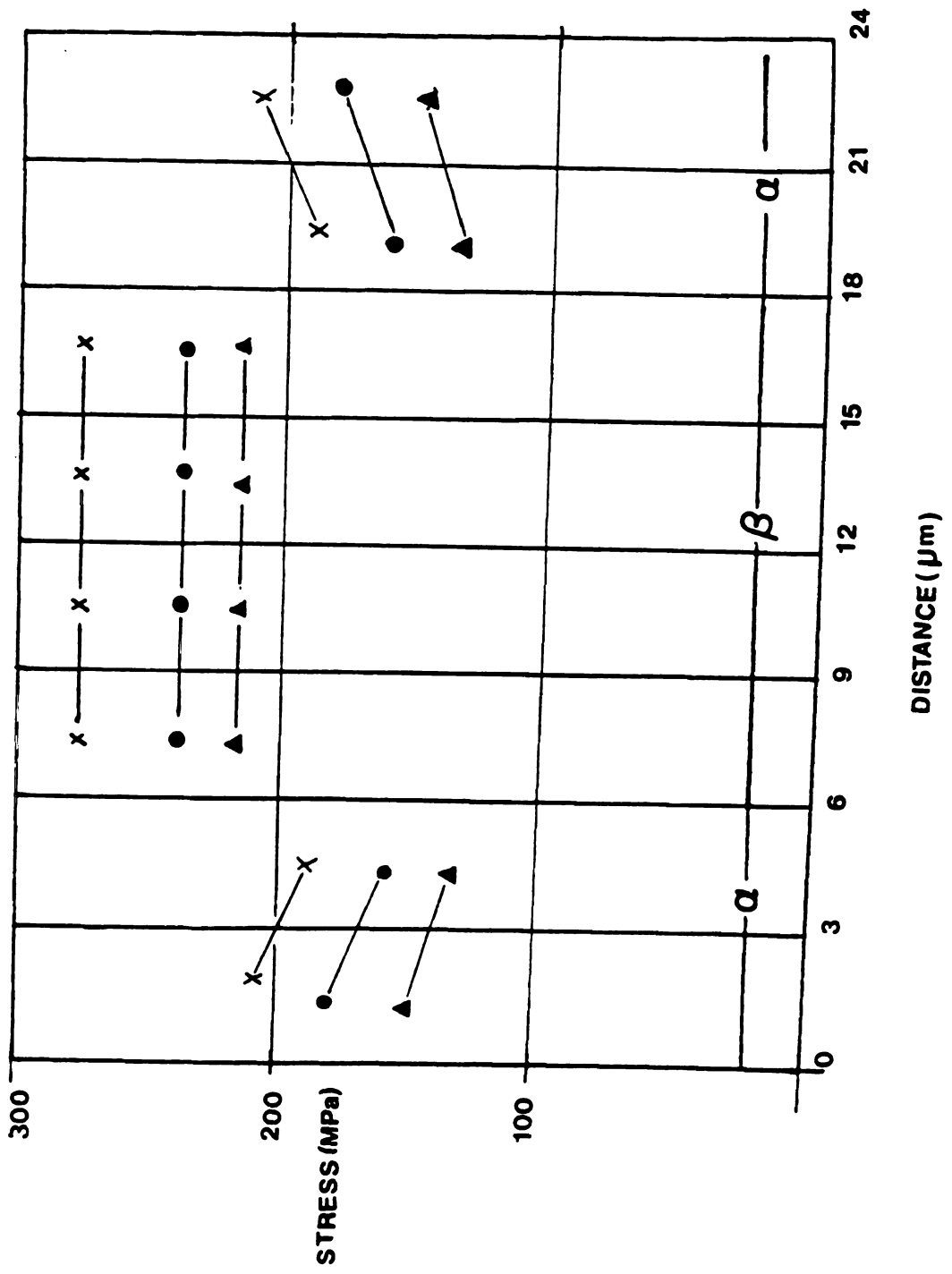




Figure 26. FEM-calculated stress distribution plot in alpha and beta region of alpha-beta brass containing 25 volume percent beta phase, in the X-direction ( $\sigma_{xx}$ ).

Applied stress level.

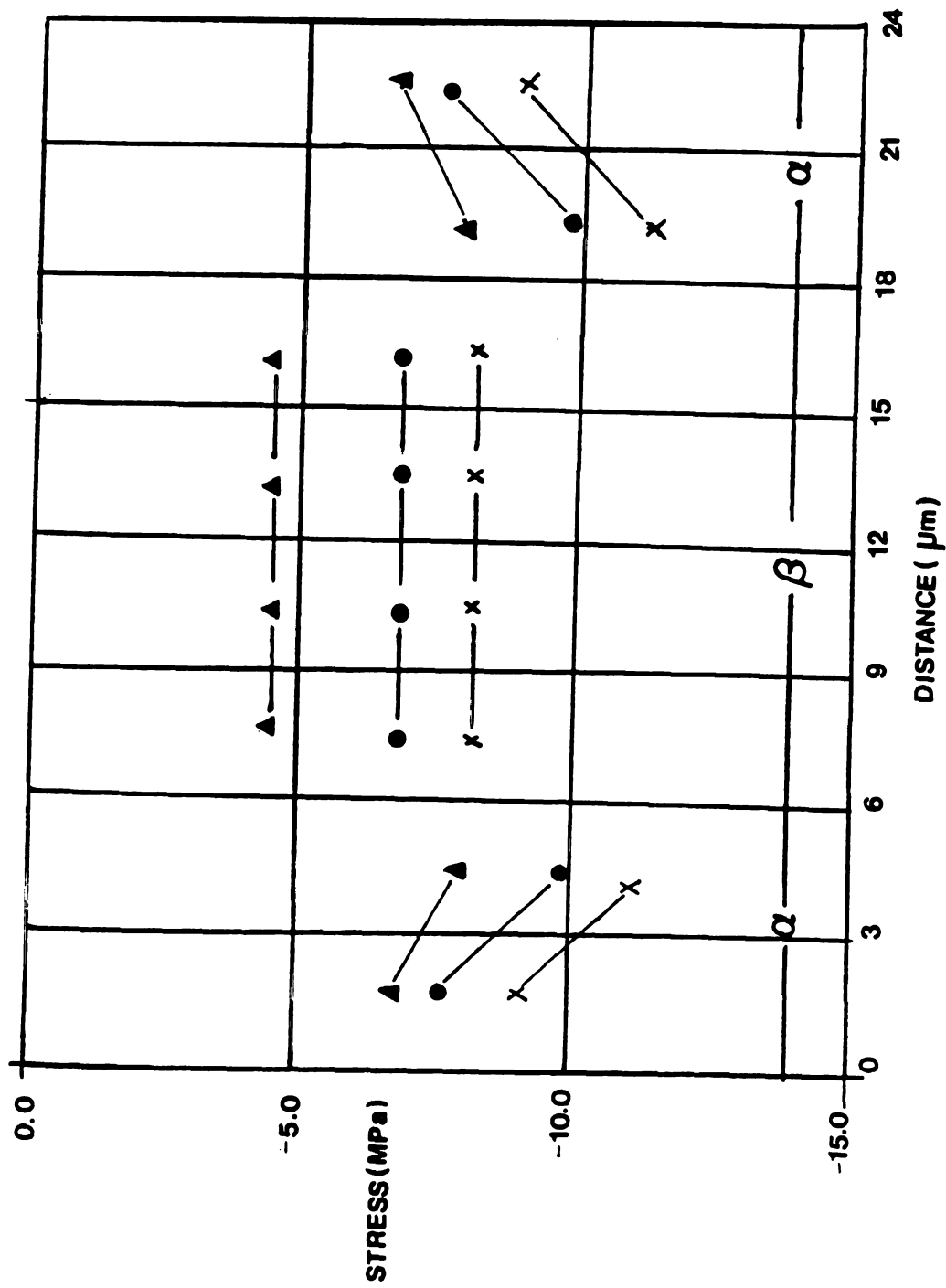
▲ 172 MPa

● 207 MPa

× 241 MPa

Grain size: small.

alpha  
ning  
ection



calculated by 60-element mesh (47) and stress and strain distributions calculated by 128-element mesh are presented in Figures 28, 29, and 30. The stress contours on the 128-element mesh used for FEM analysis are presented in Figures 31 and 32. The stress levels at different locations on the mesh are marked.

d) Stress-Strain Curve for Two-Phase Region.

Stress-strain curves for two-phase region (alpha-beta) are shown in Figures 33 and 34. At any given strain value, it is observed that the stress level for the case when tensile axis is parallel to the phase boundary is higher than for the case when the tensile axis is perpendicular to the phase boundary. Stress-strain curves for two-phase region (80 volume percent alpha, 20 volume percent beta) are shown in Figure 34. The experimentally obtained stress-strain curve was observed to be in between these two extremes (phase boundary parallel to tensile axis and phase boundary perpendicular to the tensile axis).

e) Comparison of Experimental Stress-Strain Curve With the FEM-Calculated Curves (Two Different Meshes)

The FEM-calculated stress-strain curves are at higher levels than the experimental curve. One reason could be that the input curves used for FEM analysis are themselves at higher levels than experimentally predicted curves for these materials. The curve with 128-element mesh is closer to the experimental curve than the 60-element mesh, because

Figure 27. FEM-calculated strain distribution plot in alpha and beta region of alpha-beta brass containing 25 volume percent beta phase.

Applied stress level.

X 172 MPa

● 207 MPa

▲ 241 MPa

Grain size: small.

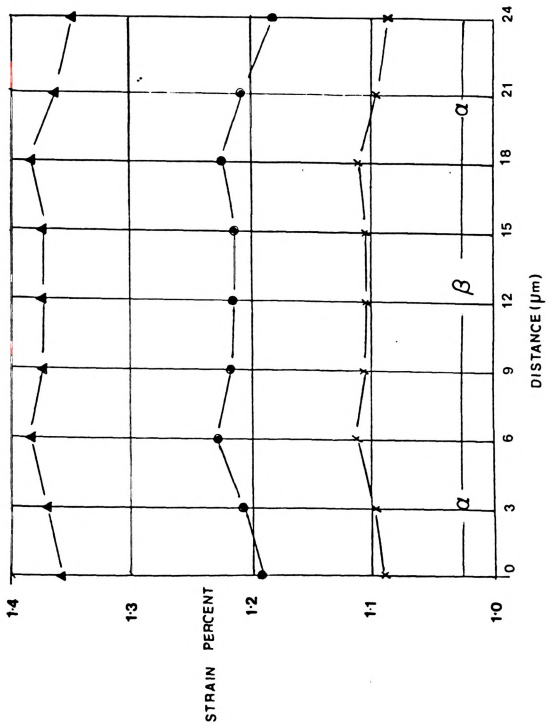


Figure 28. FEM-calculated stress distribution plot in alpha-beta region of alpha-beta brass containing 20 volume percent beta phase, in Y-direction ( $\sigma_{yy}$ ).

A) Stress distribution with 60-element mesh (Ref. 47).

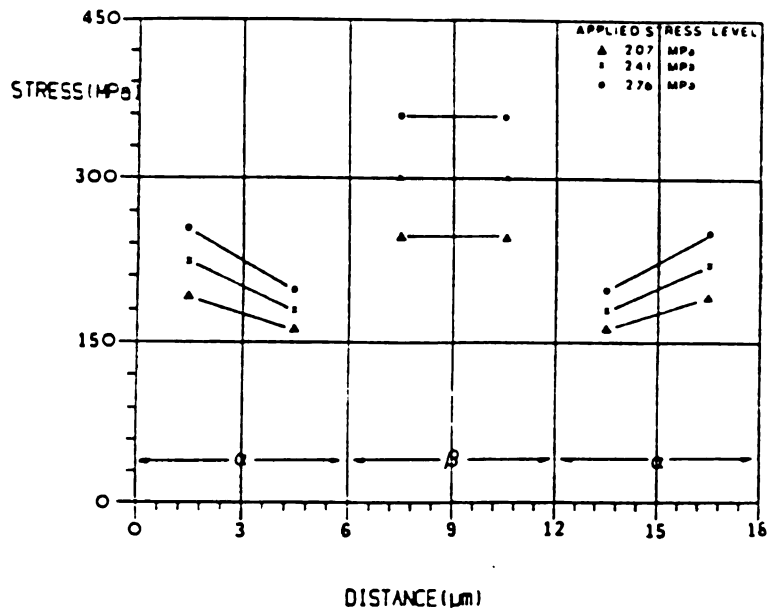
B) Stress distribution with 128-element mesh.

Applied stress level.

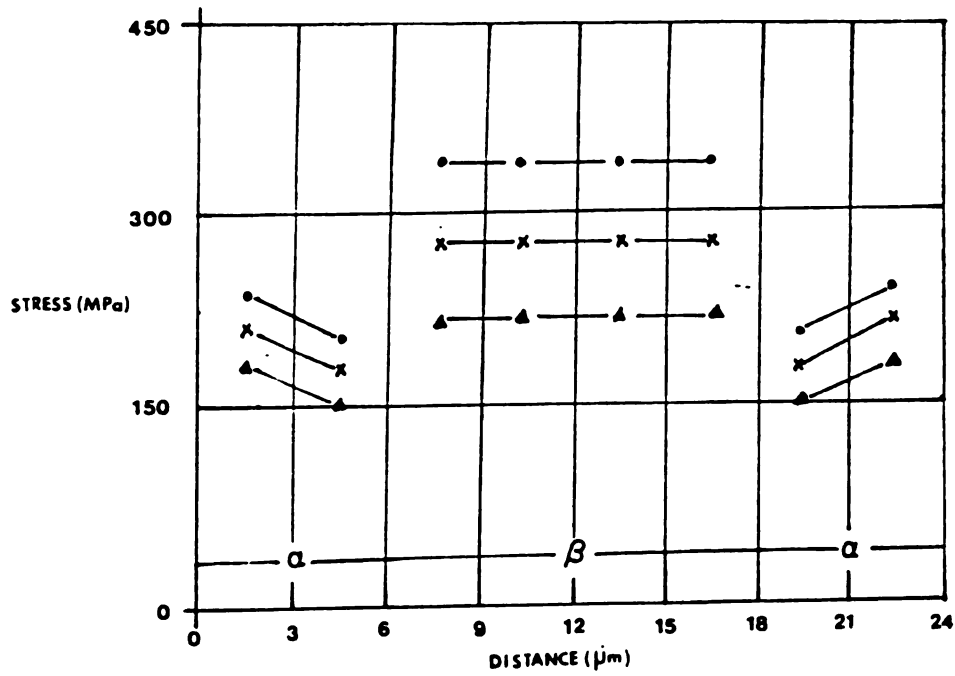
▲ 207 MPa

× 241 MPa

● 276 MPa



A



B

Figure 28. FEM-calculated stress distribution plot in alpha-beta region of alpha-beta brass containing 20 volume percent beta phase, in Y-direction ( $\sigma_{yy}$ ).

A) Stress distribution with 60-element mesh (Ref. 47).

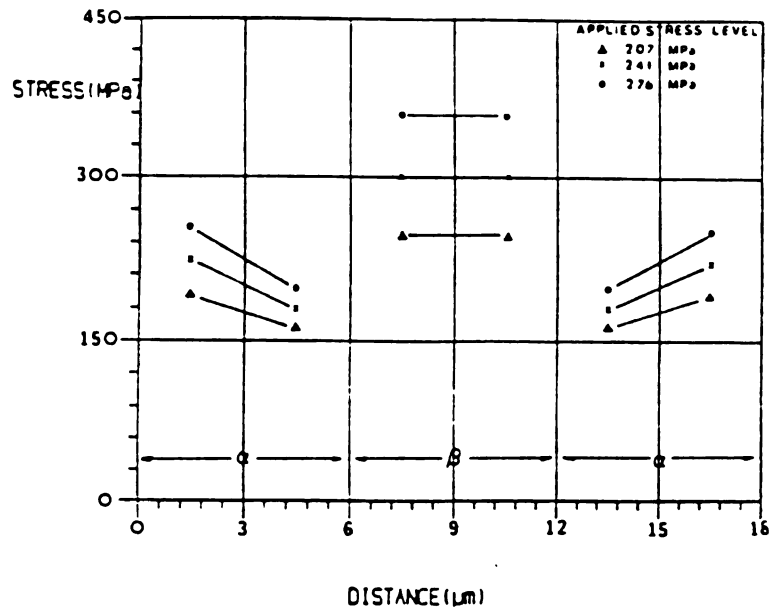
B) Stress distribution with 128-element mesh.

Applied stress level.

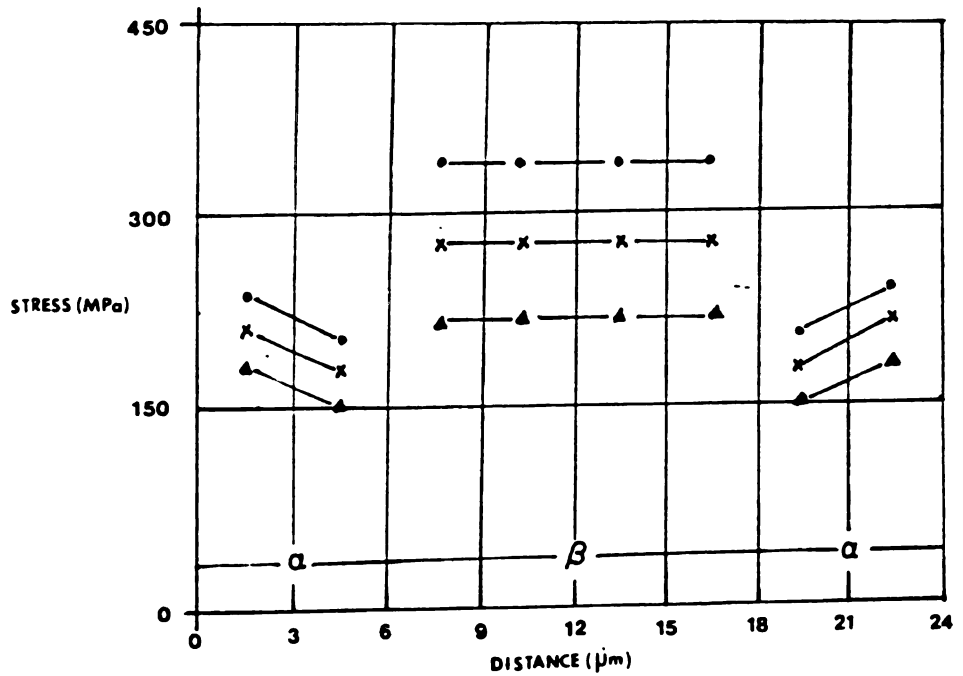
▲ 207 MPa

× 241 MPa

● 276 MPa



A



B

Figure 29. FEM-calculated stress distribution plot in alpha and beta region of alpha-beta brass containing 20 volume percent beta phase, in X-direction ( $\sigma_{xx}$ ).

A) Stress distribution with 60-element mesh (Ref. 47).

B) Stress distribution with 128-element mesh.

Applied stress level.

▲ 172 MPa

● 207 MPa

X 241 MPa

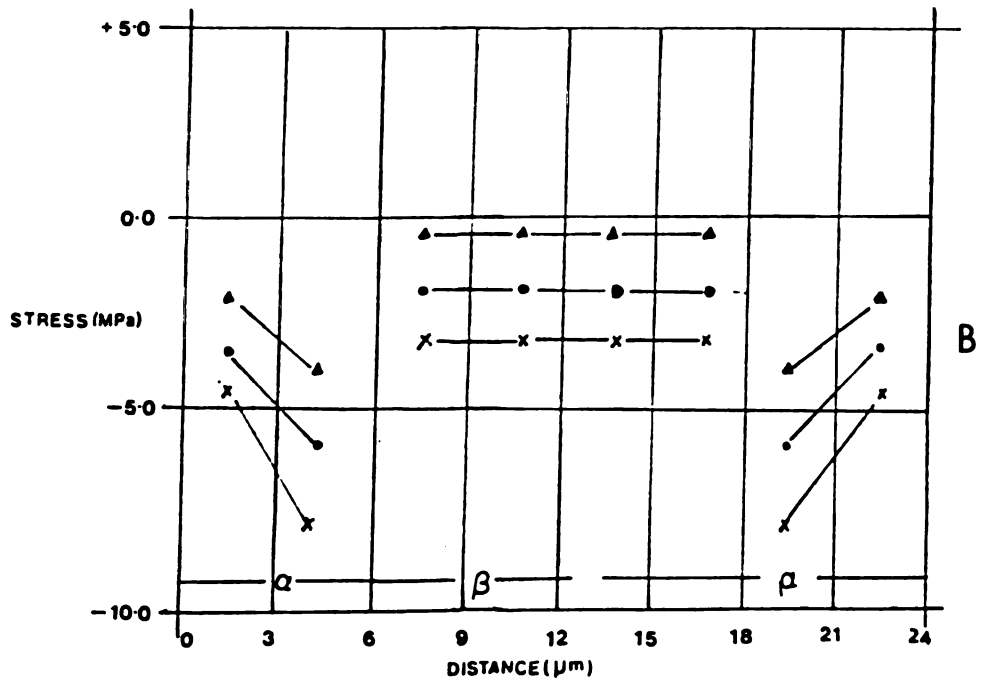
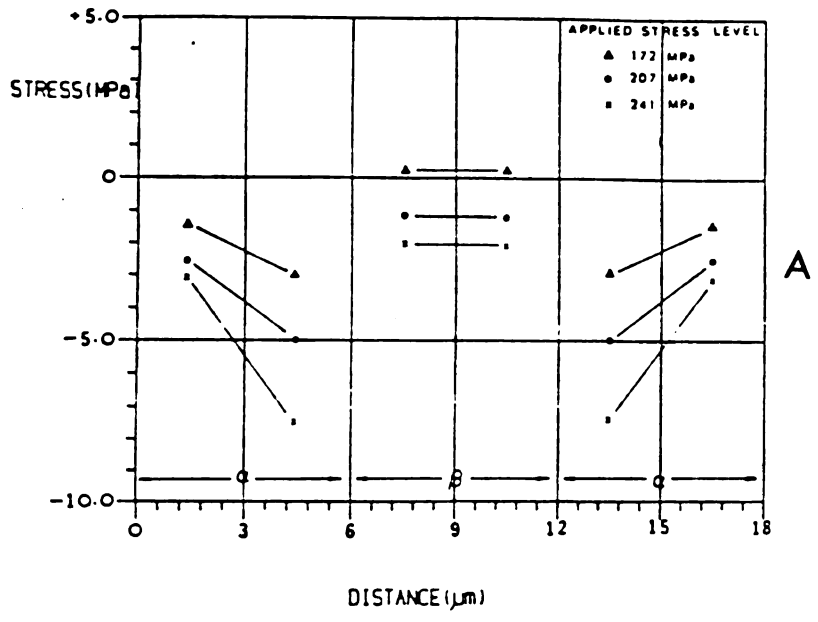


Figure 30. FEM-calculated strain distribution plot in alpha and beta region of alpha-beta brass containing 20 volume percent beta phase.

A) Strain distribution with 60-element mesh (Ref. 47).

B) Strain distribution with 128-element mesh.

Applied stress level.

X 207 MPa

● 241 MPa

▲ 276 MPa

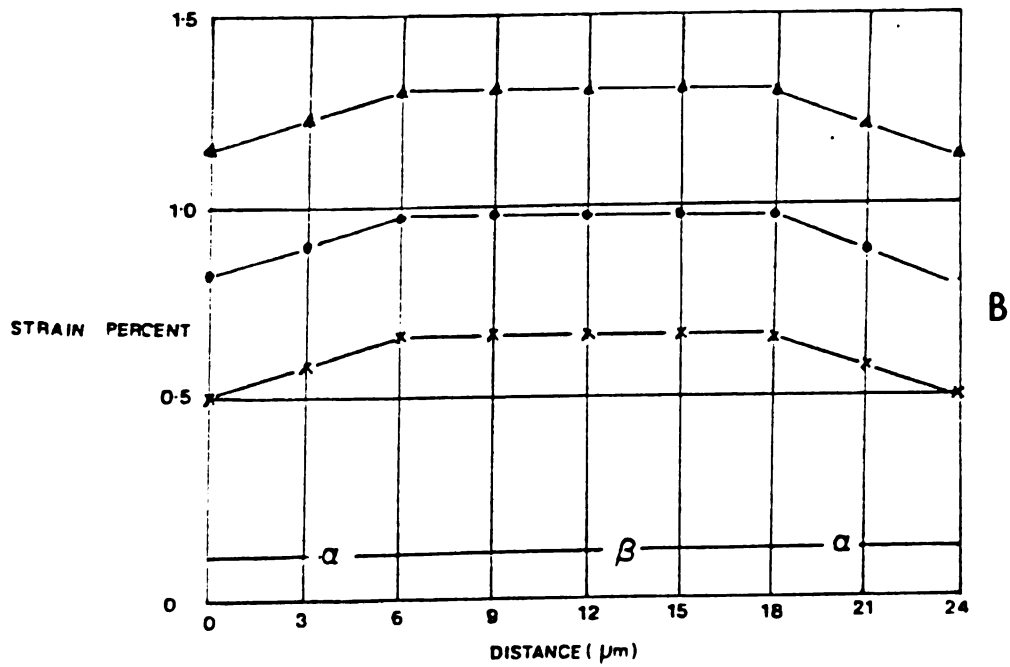
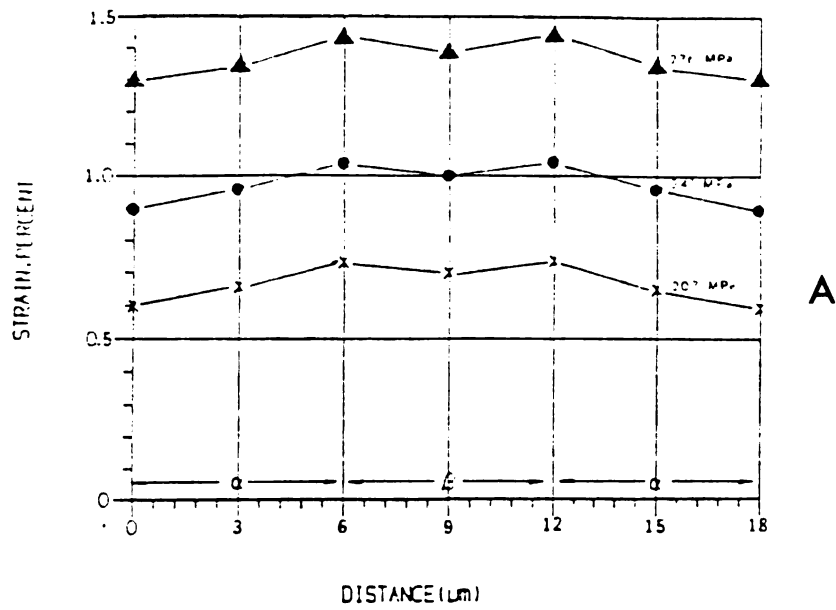
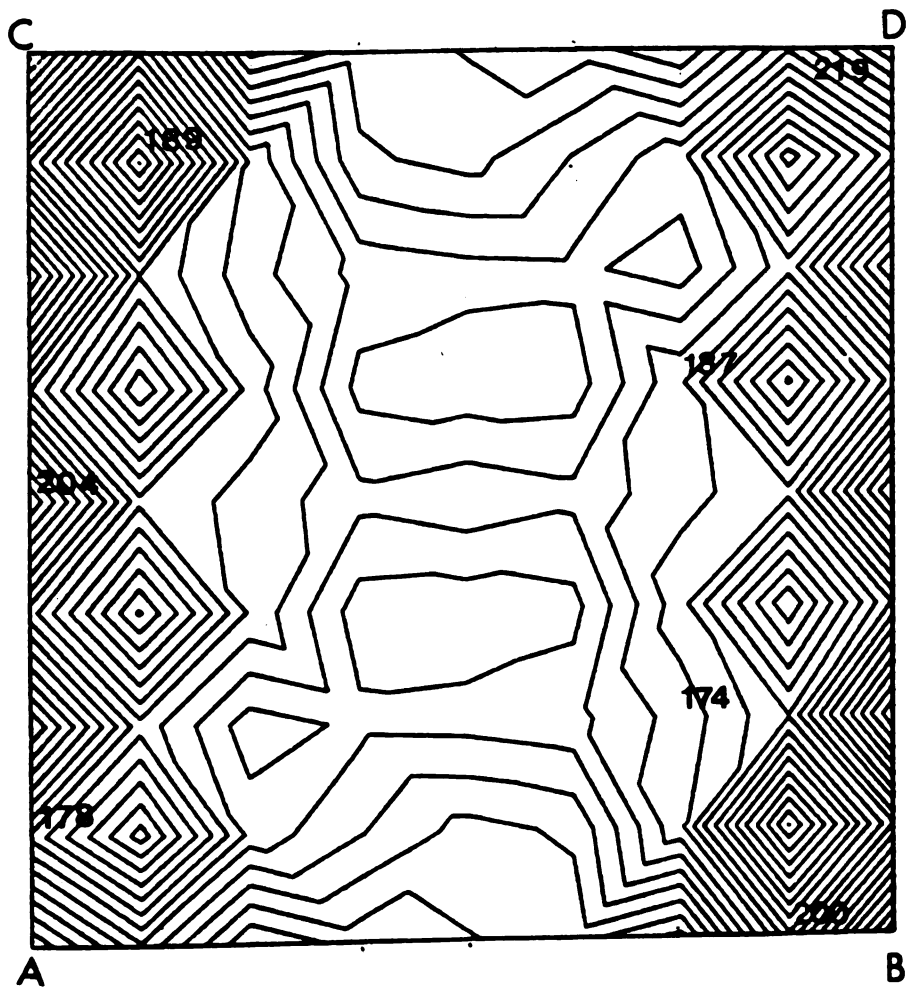


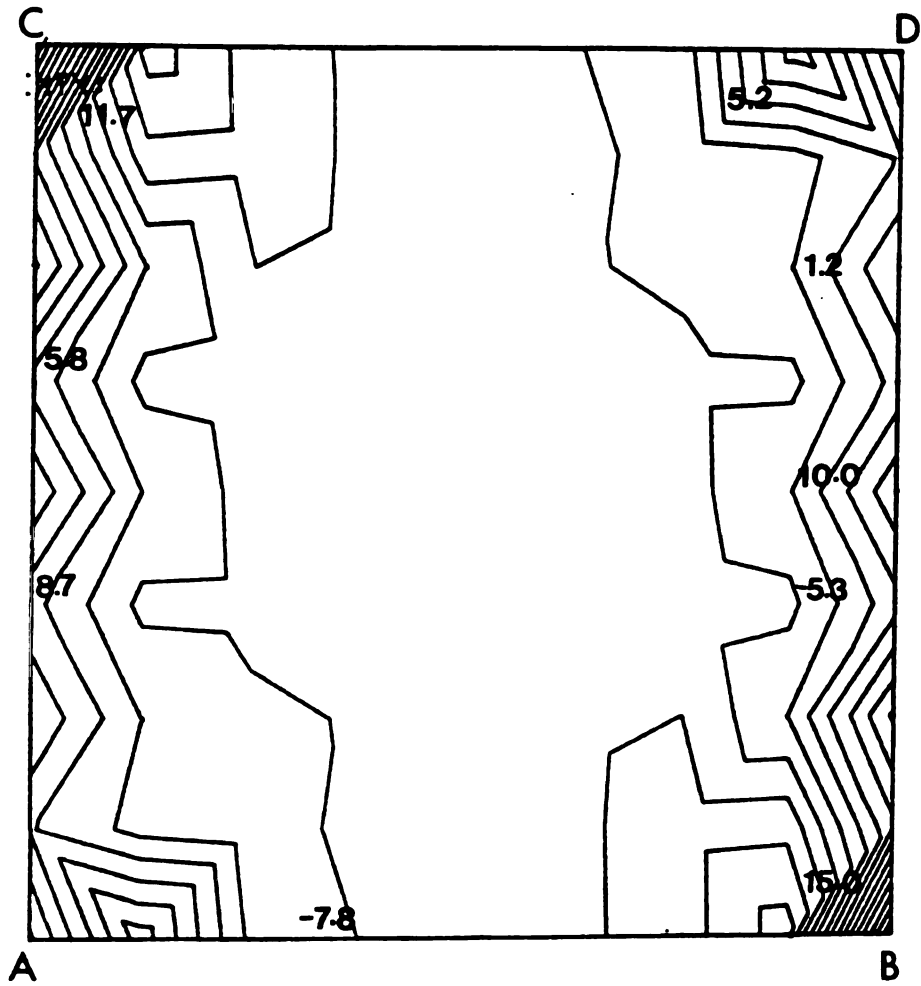
Figure 31. FEM-generated stress contours plot in the 128-element mesh for alpha-beta brass containing 25 volume percent beta phase in the loading Y-direction ( $\sigma_{yy}$ ). (The mesh levels marked are in MPa.)



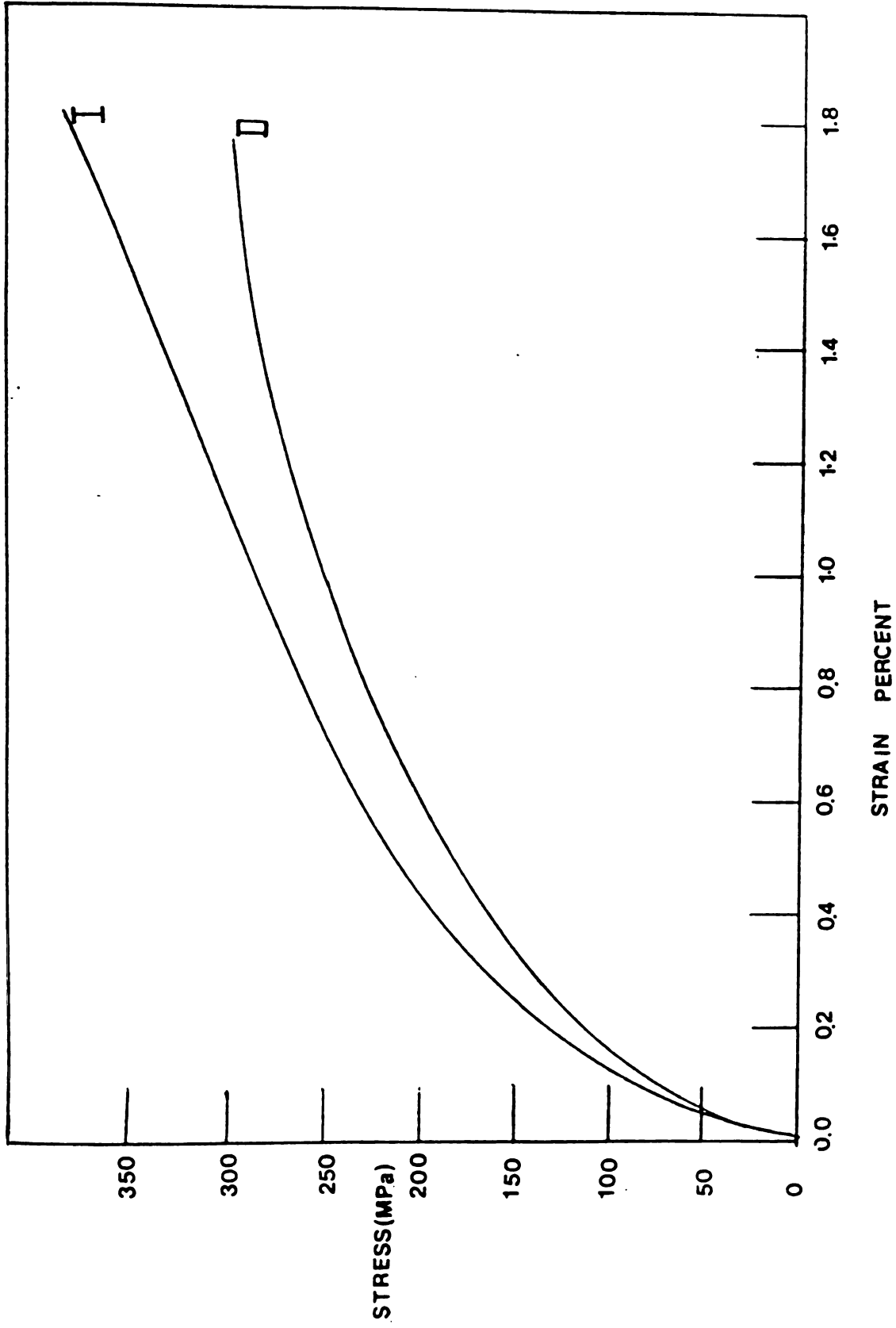
25  
in

Figure 32. FEM-generated stress contour distribution plot in the 128-element mesh for alpha-beta brass containing 25 volume percent beta phase, in the X-direction ( $\sigma_{xx}$ ). (The stress levels marked are in MPa.)

lot  
s  
the  
d



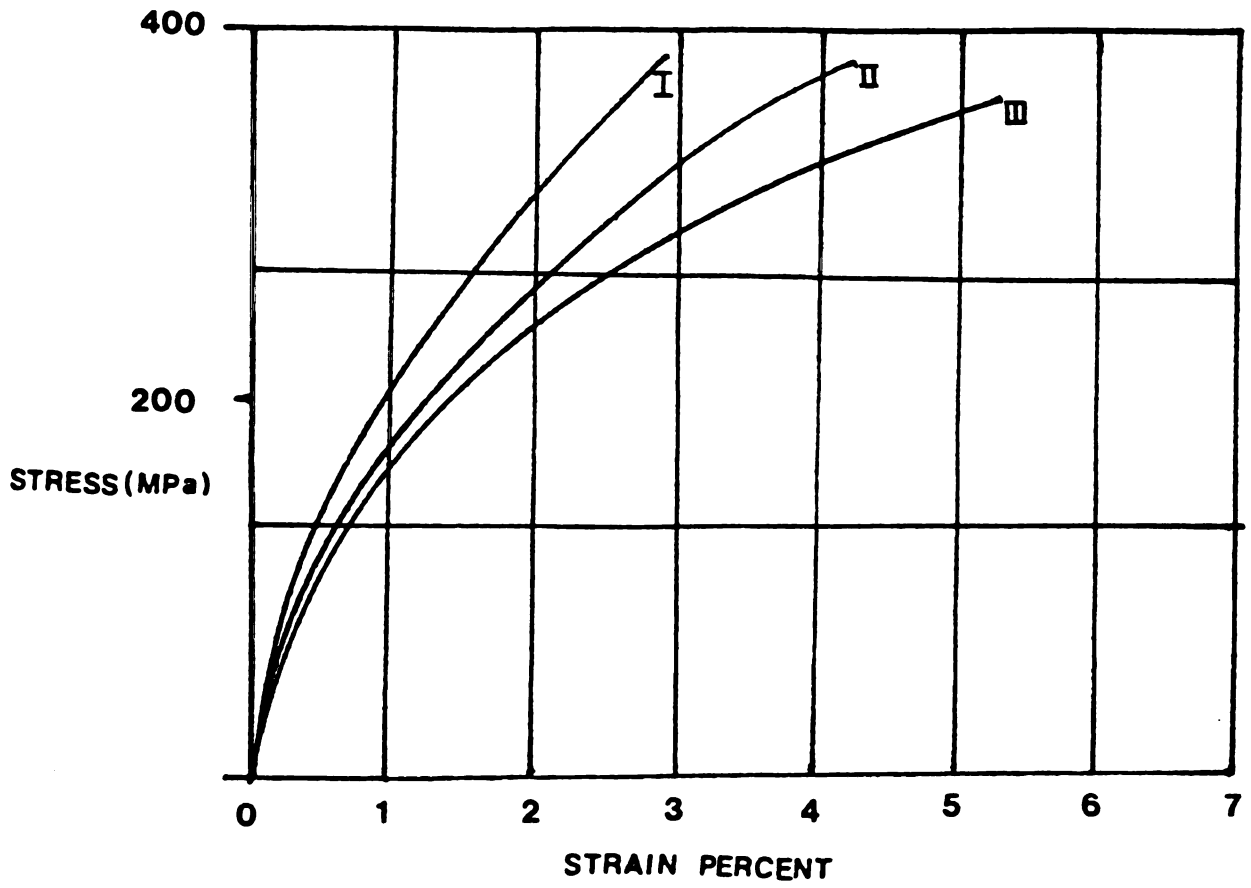
- Figure 33. FEM-calculated stress-strain curves of alpha-beta brass containing 50 volume percent of alpha and 50 volume percent beta.
- I. Phase boundary parallel to tensile axis.
  - II. Phase boundary perpendicular to tensile axis.



pha

Figure 34. FEM-calculated stress-strain curve of alpha-beta brass containing 80 volume percent of alpha and 20 volume percent beta.

- I. Phase boundary parallel to tensile axis.
- II. Experimental.
- III. Phase boundary perpendicular to the tensile axis.

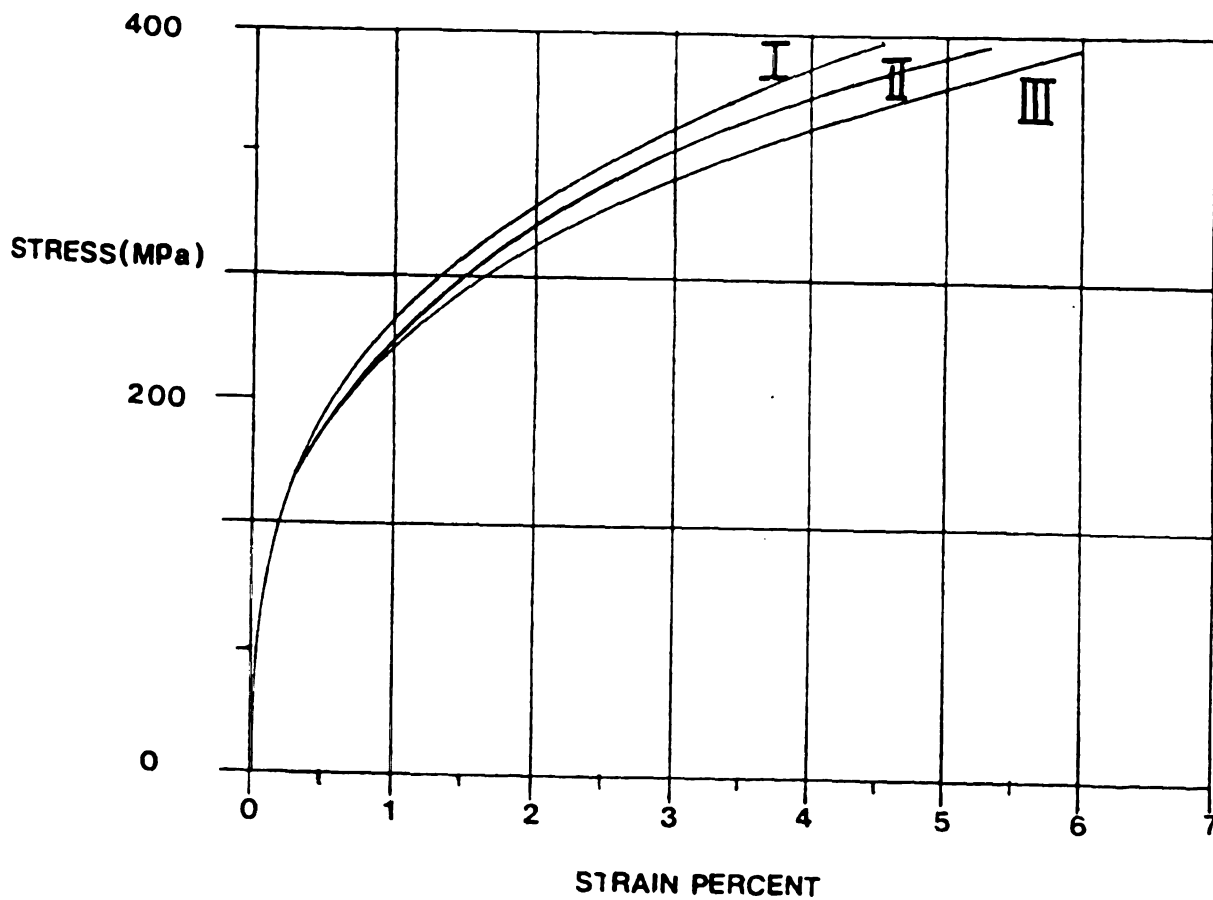


-beta  
and  
is.

the degree of accuracy has increased with more divisions in the given area. These curves are presented in Figure 35.

Figure 35. Comparison between the experimentally determined stress-strain curve of 60 Cu-40 Zn brass and the FEM-calculated curves of alpha-beta brass containing 20 volume percent beta phase.

- I. FEM curve with 60-element mesh (Ref. 47).
- II. FEM curve with 128-element mesh.
- III. Experimental.



## V. CONCLUSIONS

### V-A. Transmission Electron Microscope Studies

1. Extensive dislocation pile-ups were observed in alpha region near equiaxed phase boundary, but there was not evidence of dislocation activity due to these pile-ups in beta region for specimens that were strained up to 27 percent.

2. Slip dislocations observed in beta brass at regions away from the phase boundary were screw in character and were of type  $\frac{a}{2}\langle 111 \rangle$  gliding on  $\{110\}$ .

### V-B. FEM Analysis

1. At a specific strain it was observed that the stress level for specimens with tensile axis, parallel to the phase boundary, was higher than that for specimens with tensile axis perpendicular to the phase boundary. The experimentally obtained stress-strain curve was observed to be in between the two extremes.

2. FEM-calculated stress-strain curves attained higher stress levels for similar strain levels as compared to an experimentally obtained curve. The FEM-calculated stress-strain curve with a mesh of 128 elements was closer to the experimentally obtained one, as compared to an analysis based on 60-element mesh.

## VI. REFERENCES

1. A. Eberhardt, M. Suerey, and B. Baudalet. "Plane Interface Boundary Sliding in Alpha-Beta Brass," *Scripta Metall.*, 9, 1231 (1975).
2. A. Hingwe and K. N. Subramanian. "Deformation of Duplex Crystals and Two-Phase Bicrystals of Alpha-Beta Brass," *J. Crystal Growth*, 21, 287 (1974).
3. A. Hingwe and K. N. Subramanian. "Deformation of Duplex Crystals and Two-Phase Bicrystals of Alpha-Beta Brass," *J. Mater. Sci.*, 10, 183 (1975).
4. A. Hingwe. "Duplex Crystals and Two-Phase Bicrystals of Alpha-Beta Brass--Growth and Mechanical Properties," Ph.D. Thesis. Michigan State University (1973).
5. C. Nilsen and K. N. Subramanian. "Deformation of Alpha-Beta Brass with Oriented and Equiaxed Duplex Geometries," *Phy. Stat. Sol.*, 79, 281 (1983).
6. C. Nilsen and K. N. Subramanian. "Role of Strain Rate and Phase Boundary Geometry on Deformation Behavior of Two-Phase Bicrystals of Alpha-Beta Brass," *J. Mater. Sci.*, 19, 768 (1984).
7. C. Nilsen. "Mechanical Properties of Alpha-Beta Brass --Studies on Model Systems," Ph.D. Thesis. Michigan State University (1973).
8. A. Kezri Yazdan. "Effect of Temperature on the Deformation Behavior of Two-Phase Bicrystal of Alpha-Beta Brass," Ph.D. Thesis. Michigan State University (1973).
9. N. Fat-Halla, T. Takasugi, and O. Izumi. "On Elastic Incompatibility During the Deformation of Alpha-Beta Brass Two-Phase Bicrystals," *J. Mater. Sci.*, 15, 3071 (1980).
10. H. Kawazoe, T. Takasugi, and O. Izumi. "Fatigue of Alpha-Beta Brass Two-Phase Bicrystals," *Acta Metall.*, 28, 1253 (1980).
11. T. Takasugi and O. Izumi. "Interface Sliding in Alpha-Beta Brass Two-Phase Bicrystals," *Acta Metall.*, 28, 465 (1980).

12. T. Takasugi, O. Izumi, and N. Fat-Halla. "Activated Slip Systems During Yielding of Alpha-Beta Brass Two-Phase Bicrystals," *J. Mater. Sci.*, 13, 2013 (1978).
13. T. Takasugi, O. Izumi, and N. Fat-Halla. "Plastic Deformation and Fracture Behaviors of Alpha-Beta Brass Two-Phase Bicrystals," *Acta Metall.*, 26, 1453 (1978).
14. T. Takasugi, O. Izumi, and N. Fat-Halla. "Dynamic Observation of Fracture Phenomewnon in Alpha-Beta Brass Two-Phase Bicrystals," *J. Mater. Sci.*, 13, 2462 (1978).
15. T. Takasugi, O. Izumi, N. Fat-Halla. "Operative Slip Systems in Alpha-Beta Brass Two-Phase Bicrystals at 150K," *J. Mater. Sci.*, 14, 1651 (1979).
16. M. Hansen and K. Anderko. Constitution of Binary Alloys. McGraw-Hill, New York, p. 650 (1958).
17. R. D. Heidenreich, W. Shockley. "Electron Microscope and Electron Diffraction Study of Slip in Metal Crystals," *J. Appl. Phys.*, 5, 1029 (1948).
18. N. Brown. "The Yield Point of a Super-Lattice," *Phil. Mag.*, 4, 693 (1959)(as cited in reference 7).
19. J. P. Hirth and J. Lothe, Theory of Dislocations, McGraw-Hill, New York, p. 764 (1968).
20. E. Orwan, *Proc. Phys. Soc.*, 52, 8 (1940)(as cited in reference 8).
21. W. G. Johnston, and J. J. Gilman. Dislocations and Mechanical Properties of Crystals, Ed. Fisher. John Wiley and Sons, Inc., New York, p. 116 (1957).
22. A. L. Titchener, and W. G. Ferguson. "The Dynamic Compressive Behaviour of Beta Brass Single Crystals," *J. Inst. Metals*, 99, 1971 (as cited in reference 8).
23. D. McLean. Grain Boundary in Metals, Clarendon Press, Oxford, p. 157 (1957).
24. Y. Chung and H. Margolin. "Beta Brass Stress-Strain Relations," *Metallurg. Trans.*, 4, 1905 (1973).
25. S. Karashima. "Electron Microscope Studies of Deformed Alpha Brass, Part I--General Arrangement of Dislocations," *Trans. J.I.M.*, 2, 134 (1961).

26. S. Karashima. "Dislocation Pairs Observed in Alpha Brass," Trans. J.I.M., 3, 48 (1962).
27. W. M. Lomer, "A Dislocation Reaction in the Face-Centred Cubic Lattice," Phil. Mag., 42, 1327 (1951)(as cited in reference 8).
28. A. B. Greninger, Trans. A.I.M.E., 128, 369 (1938)(as cited in reference 7).
29. G. Ogilvie, J. Inst. Met., 81, 49 (1952-53)(as cited in reference 7).
30. A. Head, M. Loretto, and P. Humble. "Identification of Burgers Vector and Unstable Directions of Dislocations in Beta Brass," Phy. Stat. Sol., 20, 521 (1967).
31. R. W. K. Honeycombe, and W. Boas, "The Deformation and Recrystallization of an Alloy Containing Two Phases," Aust. J. Sci. Res. (A), 3, 70 (1948)(as cited in reference 7).
32. E. O. Hall. "The Luders Deformation of Mild Steel," Proc. Phys. Soc., London, B64, 747 (1951)(as cited in reference 35).
33. N. J. Petch. "The Cleavage Strength of Polycrystals," J. Iron Steel Inst., 174, 25 (1953)(as cited in reference 35).
34. A. Cottrell. Dislocation and Plastic Flow in Crystals, Clarendon Press, Oxford, p. 107 (1953).
35. Myers and Chawala. Mechanical Metallurgy Principles and Applications, Prentice-Hall, Inc., New Jersey, p. 259 (1984).
36. J. C. M. Li. "Petch Relation and Grain-Boundary Sources," Trans. TMS-A.I.M.E., 227, 239 (1963)(as cited in reference 35).
37. L. E. Murr. "TEM Observations of Dislocation Emission at Grain Boundaries in Response to Uniaxial (Tensile) Straining," Met. Trans., 6A, 505 (1975).
38. K. Tangri and T. Malis, Surface Sci., 31 (1972)(as cited in reference 35).
39. J. Jinoch, S. Ankem, and H. Margolin. "Calculation of Stress-Strain Distribution for an Alpha-Beta Ti-8Mn Alloy," Mat. Sci. Eng., 34, 203 (1978).

40. H. Fischmeister, J. Hjalmered, B. Karlsson, G. Lindon, and B. Sundstrom. Third International Conference on Strength of Materials and Alloys. Institute of Metals and Iron and Steel Institute, Cambridge and London, 1, p. 621 (1973).
41. B. Karlsson and B. Sundstrom. "Inhomogeneity in Plastic Deformation of Two-Phase Steel," Mat. Sci. Eng., 161 (1974).
42. B. Sundstrom. "Elastic-Plastic Behavior of WC-Co Analyzed by Continuum Mechanics," Mat. Sci. Eng., 12, 265 (1973).
43. S. Ankem and H. Margolin. "Finite Element Method Calculations of Stress-Strain Behavior of Alpha-Beta Ti-Mn Alloys: Part I. Stress-Strain Relations," Metall. Trans. A., 13A, 95 (1982).
44. S. Ankem and H. Margolin. "Finite Element Method Calculations of Stress-Strain Behavior of Alpha-Beta Ti-Mn Alloys: Part II. Stress and Strain Distributions," Metall. Trans. A., 13A, 603 (1982).
45. F. Monchoux, A. Rocher, J. L. Martin. "A Study of Interface Sliding at F.C.C.-B.C.C. Boundaries in a Cu-Zn Alloy," Proc. Ninth International Congress on Electron Microscopy, Ed. Martin, Toronto, 1, 422 (1978).
46. G. DeSalvo and J. Swanson. ANSYS Engineering Analysis Systems--Users Manual, 1, Swanson Analysis Systems, Inc., Houston, PA.
47. N. S. Kulkarni. "Deformation Studies on Alpha-Beta Brass," M.S. Thesis. Michigan State University (1984).
48. A. Seeger. Dislocation and Mechanical Properties of Crystals. John Wiley and Sons, New York, p. 389 (1957).

40. H. Fischmeister, J. Hjalmered, B. Karlsson, G. Lindon, and B. Sundstrom. Third International Conference on Strength of Materials and Alloys. Institute of Metals and Iron and Steel Institute, Cambridge and London, 1, p. 621 (1973).
41. B. Karlsson and B. Sundstrom. "Inhomogeneity in Plastic Deformation of Two-Phase Steel," Mat. Sci. Eng., 161 (1974).
42. B. Sundstrom. "Elastic-Plastic Behavior of WC-Co Analyzed by Continuum Mechanics," Mat. Sci. Eng., 12, 265 (1973).
43. S. Ankem and H. Margolin. "Finite Element Method Calculations of Stress-Strain Behavior of Alpha-Beta Ti-Mn Alloys: Part I. Stress-Strain Relations," Metall. Trans. A., 13A, 95 (1982).
44. S. Ankem and H. Margolin. "Finite Element Method Calculations of Stress-Strain Behavior of Alpha-Beta Ti-Mn Alloys: Part II. Stress and Strain Distributions," Metall. Trans. A., 13A, 603 (1982).
45. F. Monchoux, A. Rocher, J. L. Martin. "A Study of Interface Sliding at F.C.C.-B.C.C. Boundaries in a Cu-Zn Alloy," Proc. Ninth International Congress on Electron Microscopy, Ed. Martin, Toronto, 1, 422 (1978).
46. G. DeSalvo and J. Swanson. ANSYS Engineering Analysis Systems--Users Manual, 1, Swanson Analysis Systems, Inc., Houston, PA.
47. N. S. Kulkarni. "Deformation Studies on Alpha-Beta Brass," M.S. Thesis. Michigan State University (1984).
48. A. Seeger. Dislocation and Mechanical Properties of Crystals. John Wiley and Sons, New York, p. 389 (1957).

MICHIGAN STATE UNIVERSITY LIBRARIES



3 1293 03196 7304